

1  
2  
3  
4  
5  
6  
7  
8  
9  
10  
11  
12  
13  
14  
15  
16  
17  
18  
19  
20  
21  
22  
23  
24  
25  
26  
27  
28  
29  
30  
31  
32  
33  
34  
35

## Tunable bet hedging in yeast responses to osmotic stress

Yoshikazu Hirate<sup>1†</sup>, Samuel Bottani<sup>2</sup>, Wyming Lee Pang<sup>3‡</sup>, Suzannah Rutherford<sup>1\*</sup>

### Affiliations

<sup>1</sup>Division of Basic Sciences, Fred Hutchinson Cancer Research Center, Seattle, WA.

<sup>2</sup>Laboratoire Matière et Systèmes Complex, CNRS and Université Paris Diderot- Sorbonne Paris Cité, Paris, France.

<sup>3</sup>Department of Bioengineering, University of California San Diego, San Diego, CA.

\*Correspondence to: [srutherf@fhcrc.org](mailto:srutherf@fhcrc.org).

† Current address Center for Experimental Animals, Tokyo Medical and Dental University, 1-5-45 Yushima, Bunkyo-ku, Tokyo 113-8510, Japan.

‡ Current address UCSD Health Sciences, 9500 Gilman Drive, Department 0012, La Jolla, CA 92093-0012.

36 **Summary**

37 Microbes limit risk by stochastic bet hedging – low frequency expression of less fit, slow growing  
38 cells constitutively preadapted against many stresses including antibiotics. By contrast, here we  
39 report continuous variation in the *induced* frequency of cells with slow osmotic stress signaling,  
40 survival and proliferation among 50 ecologically-distinct strains of budding yeast challenged by  
41 sudden hyperosmotic stress. Despite extensive variation in early mortality, strains displayed  
42 robust perfect adaptation and recovery of steady-state viability in moderate stress. In severe  
43 stress survival depended on strain-specific proportions of cells with divergent strategies.  
44 ‘Cautious’ cells survived without dividing; ‘reckless’ cells attempted to divide too soon and failed,  
45 killing both mother and daughter. We show that heritable frequencies of cautious and reckless  
46 cells produce a rapidly diversifying template for microbial bet hedging that mimics natural  
47 variation in stress responses whose timing, amplitude and frequency could evolve – be ‘tuned’  
48 by – different patterns of environmental stress.

49 An ability to sense and respond appropriately to environmental challenge can mean the  
50 difference between life and death. Organisms adapt physiologically to short-term stresses and  
51 evolve to track longer-term environmental change. Environmental stress responses present  
52 since life's common ancestor are exquisitely adapted by natural selection in a diversity of  
53 habitats (Tomanek, 2010). For example heat shock proteins that allow survival of what would  
54 otherwise be killing temperatures are induced by slight elevations above optimal temperatures  
55 in thermal environments ranging from Antarctic to superheated hydrothermal vents, and have  
56 even evolved to anticipate and track predictable temperature fluctuations for organisms living in  
57 tide-pools (Feder and Hoffmann, 1999; Richter et al., 2010). By contrast, unpredictable and  
58 severe environmental stresses impose a higher-level selection over populations spanning  
59 multiple generations. Particularly for genetically related lineages or clones of microorganisms,  
60 genotypes that consistently produce a small fraction of cells with unsolicited stress responses  
61 (bet hedgers) are favored over genotypes that produce only optimally-fit individuals (Arnoldini et  
62 al., 2012; Donaldson-Matasci et al., 2013; King and Masel, 2007; Meyers and Bull, 2002). A  
63 trade-off between the growth arrest and cost of mounting unsolicited stress responses in  
64 preadapted individuals versus the potential escape from extinction for a diversified population or  
65 clone in unexpected and sudden stress favors the short term sacrifice of arithmetic mean fitness  
66 for longer-term multiplicative fitness (Arnoldini et al., 2012; De Jong et al., 2011; King and  
67 Masel, 2007; Simons, 2011). While pre-adaptive, stochastic stress resistance is a well-studied  
68 form of bet hedging in microorganisms, less is known about evolutionary forces governing  
69 physiological adaptation and the dangerous resumption of cell divisions in on-going episodes of  
70 environmental stress whose severity and duration are also often unpredictable.

71 The yeast high osmolarity glycerol (HOG) signaling pathway is central to an elaborate  
72 stress response that reduces cellular damage and death in unpredictable osmotic environments  
73 where the balance between external solutes and free water pressure in the cell can change  
74 suddenly (Hohmann, 2002). The HOG pathway consists of at least two highly-conserved, multi-  
75 component osmotic stress sensors linked to a parallel series of at least 15 kinases and  
76 accessory proteins that ultimately alter the activity of nearly 10% of the yeast genome  
77 (Hohmann, 2002; Saito and Posas, 2012). The sheer numbers of genes involved in HOG  
78 signaling, their conservation, and their elaborate circuitry suggest that a nuanced response to  
79 osmotic stress has been crucial and strongly selected throughout evolutionary history. However  
80 a main function of the HOG pathway is the production and accumulation of intracellular glycerol,  
81 which restores water balance and, as demonstrated by a large body of work from many labs, is  
82 essential for survival, physiological adaptation and proliferation in on-going hyperosmotic stress  
83 (Babazadeh et al., 2014; Clotet and Posas, 2007; Hohmann, 2002; Hohmann et al., 2007; Nadal  
84 et al., 2002; Saito and Posas, 2012). In the wild, yeast must balance immediate, individual  
85 survival against population-level evolutionary fitness. Individual fitness requires that cells  
86 carefully sense the amplitude and direction of environmental change and safely reenter the cell  
87 cycle after stress (Clotet and Posas, 2007). On the other hand, multiplicative fitness favors

88 clonal populations that respond as rapidly as possible to improved conditions with on average  
89 earlier cell cycle reentry and faster proliferation – even if some individuals that reenter the cell  
90 cycle too quickly are lost (Ratcliff et al., 2014).

91 The hyperosmotic stress response of budding yeast is almost certainly under strong  
92 selection in nature and has well-characterized and accessible signaling and phenotypic traits  
93 that can be measured in the lab, making this an ideal system is ideal for characterizing the  
94 mapping between signaling behavior and fitness (Clotet and Posas, 2007; Hohmann, 2002;  
95 Saito and Posas, 2012). For example, glycerol-3-phosphate dehydrogenase (*GPD1*) is rate-  
96 limiting for glycerol production (Remize et al., 2001). We use the synthesis and accumulation of  
97 green fluorescent protein (GFP) integrated into the gene for *GPD1* as a proxy for HOG pathway  
98 activity (*GPD1::GFP*). To our knowledge bet hedging and developmental noise have been  
99 exclusively studied among cells or micro-colonies of a single or few strain backgrounds. Here  
100 we characterize natural variation in osmotic stress signaling, survival and adaptation in both  
101 exponentially growing and nearly quiescent cultures of diploid yeast. To that end we used a  
102 synthetic population of diverse yeast genotypes made by crossing *GPD1::GFP* in the genetic  
103 background of a standard laboratory strain (BY4742 *MAT $\alpha$* ) to a panel of wild and industrial  
104 genetic backgrounds –e.g. fifty different haploids of the opposite mating type extracted from  
105 globally diverse, sequence-validated strains of *Saccharomyces cerevisiae* deposited to the  
106 collection of the Royal Netherlands Academy of Arts and Sciences over the past 100 years  
107 (CBS; Table 1 and supplement).

108  
109

## 110 **Results**

111

### 112 **Osmotic stress responses of rapidly dividing cultures**

113 The behavior of single cells before and after their exposure to osmotic stress was followed in  
114 several strains by time-lapse video microscopy of monolayer cultures in custom microfluidics  
115 devices (Bennett et al., 2008). When cells in exponential growth were exposed to sudden  
116 hyperosmotic stress, cell volume decreased, cell division and budding immediately stopped, and  
117 daughter cells retracted (Miermont et al., 2013). After a lag period proportional to the severity of  
118 the stress GFP fluorescence driven by the *GPD1* promoter began to accumulate in the  
119 cytoplasm of surviving cells. Cells that did not accumulate *GPD1::GFP* to high levels did not  
120 survive or adapt, developed large vacuoles, and began to die, remaining in view as shrunken  
121 cell ghosts. As GFP accumulated to saturation levels in the surviving cells, they adapted to the  
122 higher osmotic pressure, resumed cell division, budded and began to divide with a longer half  
123 time, producing daughter cells with similarly high fluorescence (Miermont et al., 2013). On the  
124 other hand, we measured the viability of each culture and *GPD1::GFP* accumulation per cell  
125 using flow cytometry of statistically large numbers of cells from all 50 strains (~10,000 cells /  
126 sample). The rate and extent of mean *GPD1::GFP* accumulation in exponentially growing

127 cultures exposed to hyperosmotic media depended on the severity of the stress and the genetic  
128 background of each strain (Figure 1A). Prior to the osmotic stress mean *GPD1::GFP*  
129 fluorescence and viability were uncorrelated. After 2 hours in moderate 0.75 M KCl viability  
130 decreased and became steeply correlated with accumulated *GPD1::GFP* (Figures 1B and C).  
131 As expected, natural variation in the strength of HOG signaling was directly responsible for  
132 variation among the strains in osmotic stress survival.

133

### 134 **Negative feedback drives a robust recovery**

135 The initially strong positive correlation between variation in *GPD1::GFP* accumulation and  
136 variation in viability reversed as cells adapted and began to divide (Figure 1C; 4 hours). This  
137 distinguished an early phase (0 – 2 hours) of the response when viability decreased markedly  
138 and acute HOG signaling promoted osmotic stress survival and a later phase (2 – 4 hours)  
139 when viability recovered but became negatively correlated with HOG signaling and *GPD1::GFP*  
140 accumulation. The switch from positive to negative correlations might have indicated that  
141 stronger HOG signaling, initially beneficial, suddenly caused lower viability. However, negative  
142 feedback controls, occurring at many levels and timescales, are present in essentially all of the  
143 varied mechanisms that act in concert to increase intracellular glycerol and restore water  
144 balance. We think it more likely that negative feedback increased signaling in the surviving cells  
145 of the less viable strains. For example (1) unequal water pressures activate osmotic stress  
146 sensors, glycerol channels and other pressure-sensitive components whose activities control  
147 and depend on water balance (e.g. see Figure 5 in Hohmann 2002 (Hohmann, 2002; Saito and  
148 Posas, 2012)), (2) *GPD1* indirectly controls and is controlled by osmotic stress-sensitive kinases  
149 that respond to upward and downward changes in water balance (Lee et al., 2012), and (3)  
150 nuclear Hog-1 MAP kinase increases the transcription of phosphatases that restore its own  
151 cytoplasmic localization and basal activity (Jacoby et al., 1997; Muzzey et al., 2009; Wurgler-  
152 Murphy et al., 1997).

153 Consistent with acting negative regulation, there was a strong and highly significant  
154 correlation between early mortality (0 – 2 hour decreases in viability) and later accumulations of  
155 *GPD1::GFP* (2 – 4 hours; Table 2). We reasoned that cells and strains that adapt quickly  
156 experience lower and less sustained effects of osmotic stress (e.g. water loss) with more rapidly  
157 attenuated HOG pathway activity and lower *GPD1::GFP* accumulation. Conversely, surviving  
158 cells of strains that were slower to adapt and less viable would experience higher and more  
159 sustained osmotic (and likely other) stress(es). Prolonged osmotic stress would maintain HOG  
160 signaling and *GPD1* transcription – which is also activated by general stress responses (Boy-  
161 Marcotte et al., 1998) – further promoting *GPD1::GFP* accumulation (e.g. a negative feedback  
162 regulation of viability by general stress responses). Indeed, even as *GPD1::GFP* and viability  
163 became negatively correlated, their *rates of change* remained positively correlated (Figure 1C, 2  
164 – 4 hours and insets; Table 2), prompting a parsimonious interpretation that osmotic stress

165 signaling promotes adaptation and viability during both the initial and recovery phases of the  
166 response.

167 By 4 hours all strains had adapted to a new steady state in 0.75M KCl and later  
168 viability remained largely unchanged (Figure 1C inset, lower right). Interestingly, initial  
169 decreases in steady-state viability (0 – 2 hour mortality) were almost perfectly restored by 4  
170 hours (Figure 1D) and, remarkably, by 6 hours early mortality and recovery were over 98%  
171 correlated ( $R^2 = 0.9852$ ,  $P < 0.0001$ ,  $N = 18$ ; see legend Figure 1D). The biological robustness of  
172 adaptation and complete recovery of steady state viability further support the idea that negative  
173 feedback restores viability through continued activation of stress responses. Indeed, the  
174 continued accumulation of *GPD1* and glycerol – directly responsible for restoration of water  
175 balance and reduction of osmotic stress – suggests that intracellular glycerol concentrations  
176 integrate the cumulative activities of many facets of the osmotic stress response (e.g. provides a  
177 plausible biological mechanism for “integral feedback” that virtually assures perfect  
178 adaptation (Muzzey et al., 2009; Yi et al., 2000); manuscript in review). However, despite their  
179 resilience, strains that were relatively slower to adapt would be ultimately less fit than rapidly  
180 adapting strains due to their higher death rate, slower recovery, and lower viabilities before and  
181 after adaptation.

182

### 183 **Extreme stress resistance of older cultures**

184 By contrast with exponential cultures, when the aging yeast cultures (post-diauxic) were  
185 exposed to hyperosmotic media they survived and adapted after long periods in unprecedented  
186 conditions (Movies 1 and 2). As aging cultures deplete available glucose in their media they  
187 undergo a metabolic change called the diauxic shift (Galdieri et al., 2010). During post-diauxic  
188 growth stress response proteins accumulate, cell division slows and then stops, and cells enter  
189 quiescence (Gray et al., 2004). Remarkably, post-diauxic cultures survived up to 5 weeks in 3 M  
190 KCl (41/50 strains). They could not adapt and did not grow in 3 M KCl, but recovered rapidly  
191 and grew when plated on fresh isotonic media (Figure 2B). When we tested their limits of  
192 adaptation in increasing concentrations of KCl all but one strain could grow on 2.6 M KCl media  
193 and three strains could grow on media containing 2.9 M KCl (Table 3). We are unaware of  
194 previous reports of such extreme osmotic stress survival or adaptation limits for budding yeast of  
195 any growth stage or genotype.

196

### 197 **Heterogeneity of cells in older cultures**

198 By contrast with cultures in exponential growth, in post-diauxic growth the genetically identical  
199 cells within each strain and culture were surprisingly heterogeneous in their size, shape and  
200 signaling behaviors (Figure 2). Neither total *GPD1::GFP* fluorescence nor rates of change in  
201 fluorescence was strongly correlated with viability. After several hours in 2.5 M KCl,  
202 *GPD1::GFP* increased sharply in one group of cells as they began to divide. More surprising,  
203 another group of cells induced *GPD1::GFP* to high levels, started to divide and then popped,

204 killing both the mother and daughter (Movie 3). Other cells had slower signaling and cell division  
205 while the most 'cautious' groups of cells failed to signal or divide but remained in a cellular state  
206 of static viability without dividing.

207         The unique signaling trajectories of most strains were highly reproducible. We used  
208 machine learning to assign the different behaviors of the cells in each sample to four Gaussian  
209 distributions ( $G_0$ - $G_3$ ) described by eight parameters – means and covariances – numbered  
210 according to their increasing levels of fluorescence (Figure 2–figure supplement 1). Only the  
211 mean level of *GPD1::GFP* pre-accumulated into cells of the  $G_3$  distribution of each strain during  
212 post-diauxic growth – *prior* to the osmotic challenge and therefore unrelated to osmotic stress  
213 signaling – predicted survival at any time. The amount of *GPD1::GFP* in  $G_3$  cells at time 0  
214 predicted early but not later viability and this relationship was better fit by 2<sup>nd</sup> order quadratic  
215 rather than linear functions of *GPD1::GFP* (Table 4), showing that early survival was higher in  
216 strains with intermediate  $G_3$  accumulations (more variation explained and lower mean square  
217 errors). Despite the fine-scaled characterization of osmotic stress signaling behaviors of the  
218 different groups of cells in each strain, none of the distributions learned by the Gaussian mixture  
219 model, neither pre-accumulated  $G_3$ , total *GPD1::GFP* fluorescence, nor stress-induced  
220 *GPD1::GFP* in any distribution, embodied features of osmotic stress signaling important for later  
221 survival.

222

### 223 **Continuous variation in stress responses**

224 In order to map osmotic stress-responsive signaling onto survival more directly, we clustered  
225 the osmotic stress signaling trajectories of each strain using state vectors to describe directly  
226 *GPD1::GFP* distributions of cells in each culture unbiased by Gaussian assumptions or  
227 approximations. Based on their shared and strain-specific (heritable) signaling behaviors, the 50  
228 strains rapidly converged onto two large groups made up of six mean clusters (Figure 2). Each  
229 strain was further ordered within and between mean clusters based on their clustering statistics  
230 (Table 5), with their rank order describing increasingly rapid accumulations of *GPD1::GFP* and  
231 'reckless' signaling (Figure 2-figure supplement 2). Tellingly, both mean cluster (Figure 3B) and  
232 rank (Figure 3C) predicted viability over time (Table 4), thereby confirming the biological  
233 relevance of 'cautious' versus 'reckless' osmotic stress signaling, validating our clustering  
234 method and supporting the role of natural osmotic stress signaling differences between strains  
235 in shaping variation in fitness during osmotic stress.

236

### 237 **Evidence for bet hedging**

238 As cautious and reckless behaviors were found both within and between strains, we wondered  
239 whether bet hedging, the expression of alternate, conditionally-adaptive phenotypes within a  
240 clone of genetically identical organisms, could explain the observed variation in osmotic stress  
241 signaling and survival (King and Masel, 2007; Meyers and Bull, 2002; Philippi and Seger, 1989;  
242 Ratcliff et al., 2014; Simons, 2011). By contrast with previously described stochastic bet

243 hedging, where pre-adapted stress-resistant cells occur at generally low frequencies in clonal  
244 populations (De Jong et al., 2011; Levy et al., 2012), ranked signaling responses induced by  
245 osmotic stress were uncorrelated with the pre-adapted ( $G_3$ ) resistance acquired during post-  
246 diauxic growth and already present at time 0. Strain viabilities varied depending on their rank  
247 and the severity of the osmotic environment (Table 4). Milder conditions favored higher-ranked  
248 strains with more aggressive osmotic stress signaling strategies, but with increasing time and  
249 harsher conditions more cautious strains and behaviors became more fit. For example, W178 at  
250 rank 50 was most viable in moderate 0.75 M KCl, but the optimum shifted to rank 25 after 20  
251 hours in 2.5 M KCl, 20 after 72 hours, and 9.6 after 168 hours (1 week). After 168 hours,  
252 viability had decreased most among the most reckless, highest-ranked strains (Figures 3B and  
253 C). To confirm that the increasing survival of cautious strains was correlated with their  
254 experience of osmotic stress and not simply time in culture, we again incubated cultures in 2.5  
255 M KCl for 168 hours, but they were first exposed to a mild pre-stress (2 hours in 0.5 M KCl) to  
256 pre-induce osmotic stress proteins. If optimum rank depended solely on time in high KCl, e.g.  
257 independent of the degree of stress “experienced” by the different strains, then it should be  
258 unaffected by the short pre-stress. However, optimum rank shifted toward more reckless  
259 behaviors (rank 9.6 to rank 18;  $P < 0.0001$ ) and viability increased by ~10% in response to the  
260 pre-stress. This suggests pre-treated cells experienced lower osmotic stress and that the stress  
261 itself directly determined the optimum signaling behavior. The strong correlation between  
262 relative fitness and signaling behavior with increasing osmotic stress (see below) provides  
263 strong empirical evidence for bet hedging (Simons, 2011).

264 After 168 hours in 2.5 M KCl, the most reckless cells in the highest-ranking strains  
265 began to selectively die and disappear. For example, among replicate cultures of strain W242  
266 (rank 49) those with lower viability had fewer cells with high accumulations of *GPD1::GFP*,  
267 smaller  $G_3$  distributions, and correspondingly larger distributions of cells with lower mean  
268 *GPD1::GFP* (Figure 3D). A selective loss of cells with the highest accumulations of *GPD1::GFP*  
269 could indicate that *GPD1::GFP* levels simply decrease over time. However,  $G_3$  distributions  
270 were stable over most time points and in most strains (e.g. Figure 2-figure supplement 1). We  
271 think it more likely that after 168 hours the most aggressive cells attempted to divide and  
272 popped (as in Movie 3), preferentially decreasing the  $G_3$  distribution relative to the other  
273 distributions. Rapid signaling, adaptation and recovery of cell division, a fitness advantage in  
274 mild conditions, becomes a liability in severe or prolonged osmotic stress. On the other hand,  
275 static viability would dramatically reduce evolutionary fitness in normal environments but would  
276 allow more cautious cells and strains to survive extreme hyperosmotic stress.

277

## 278 **Evolution of bet hedging**

279 As cautious and reckless strains reliably express a range of cells with different behaviors and  
280 fitness depending on the environment, we wondered whether a simple, 2-state bet hedging  
281 model including heritable proportions of cautious and reckless cell types could account for the

282 observed variation in osmotic stress signaling and explain the complex relationship between  
283 rank and viability. Assuming aggressive osmotic stress signaling with rapid recovery and  
284 resumption of growth is the default, ancestral behavior, we hypothesized a heritable probability  
285 of cautious signaling and behavior arose in response to the unpredictable severity and duration  
286 of potentially lethal osmotic environments. To test this idea, we modeled the relative fitness of  
287 strains with different signaling strategies after several generations of growth, including abrupt  
288 changes between three osmotic stress environments that discriminate cautious versus reckless  
289 behavior. These were: (E0) a permissive environment in which both cautious and reckless cells  
290 grow equally well, (E1) a restrictive environment approximating moderate osmotic stress where  
291 reckless cells divide and cautious cells survive without dividing, and (E2) a killing osmotic stress  
292 where reckless cells die and cautious cells survive without cell division.

293 We modeled a heritable probability of daughters with cautious signaling and behavior  
294 and asked whether it could evolve ( $P: 0 \leq P \leq 1$ ). Our model calculates the relative fitness (cell  
295 numbers) of different strategies after several generations under each of the 9 possible  
296 environmental shifts between the three different selective environments (Figure 3E). Most  
297 combinations of environments favor an optimum strategy of either all cautious ( $P = 1$ ) or all  
298 reckless cell types ( $P = 0$ ). Strictly intermediate strategies and bet hedging ( $P: 0 < P < 1$ )  
299 prevailed only when the osmotic environment changed from moderate to more severe (E1  $\rightarrow$   
300 E2) with the optimum strategy  $P$  depending on the number of generations in the first  
301 environment. Shorter lag periods – corresponding to less severe osmotic conditions – and more  
302 cell divisions in E1 initially favor lower  $P$  and a higher proportion of reckless cells. Longer lag  
303 periods – corresponding to more severe conditions and fewer cell divisions – favor higher  $P$  and  
304 more cautious cells. Such worsening conditions are common in nature (for example, during  
305 fermentation or on drying fruit). Indeed, as predicted by the model, we observed that lower-  
306 ranked strains with more cautious signaling behaviors, longer lag periods and fewer attempted  
307 cell divisions were increasingly fit over time in an increasing severity of osmotic stress. This  
308 simple model provides a conceptual framework for understanding how a heritable frequency of  
309 bet hedgers can be tuned by evolution in different patterns of environmental stress.

310

## 311 **Discussion**

312 In order to understand the evolutionary trajectories of populations and species we need to  
313 understand the effects of natural genetic variation on mechanisms of development and  
314 expression of phenotypic variation. Mapping genetic variation to the spectrum of attributes and  
315 behaviors upon which selection acts defines population-level properties such as evolvability (the  
316 capacity to evolve), robustness or canalization (the capacity to withstand genetic and  
317 environmental perturbation), and norms of reaction (optimization, within a given genotype, of  
318 phenotypic responses to different environments) (Kirschner and Gerhart, 1998; Meyers and  
319 Bull, 2002; Rutherford, 2000; West-Eberhard, 2003). Predictive plasticity, the ability to sense  
320 and respond appropriately to environmental challenge is a hallmark of environmental stress

321 responses. On the other hand, diversified bet hedging, the stochastic expression of phenotypic  
322 diversity, arises when environmental signals preceding lethal stresses are unreliable or sudden.  
323 Recent theoretical papers discuss ecological forces that favor the evolution of predictive  
324 plasticity and diversified bet hedging strategies (Arnoldini et al., 2012; Donaldson-Matasci et al.,  
325 2013).

326 Bet hedging in microorganisms was originally thought to arise almost exclusively through  
327 stochastic switching of a small fraction of cells independent of environmental cues (Levy et al.,  
328 2012; Ratcliff et al., 2014). However a recent survey of morphological variation among  
329 genetically identical cells from 34 different yeast strains demonstrates that differences between  
330 strains and traits in phenotypic noise is genetically encoded and if adaptive, could therefore  
331 evolve (Yvert et al., 2013). Here we report that even when yeast cells can sense and respond  
332 appropriately to unexpected episodes of environmental stress – a classic form of predictive  
333 plasticity – to safely resume cell division they must also anticipate the imperfectly known  
334 trajectory and duration of environmental change. The yeast osmotic stress response thus  
335 combines predictive plasticity with generation of phenotypic diversity and bet hedging to  
336 optimize how aggressively and over what time course osmotic stress responses unfold.  
337 Indeed, the theoretical models predict the entanglement of plastic developmental responses  
338 with bet hedging and circumscribe the ecological settings under which they would evolve  
339 (Arnoldini et al., 2012; Donaldson-Matasci et al., 2013). The first known example of combined  
340 predictive plasticity and bet hedging in a microorganism is the starvation response of the  
341 bacteria *S. meliloti* which induces the production of 2 different daughter cells, one suited to  
342 short-term starvation and the other suited to longer-term starvation (Ratcliff and Denison, 2010).  
343 Also consistent with our results are recent laboratory evolution studies showing that (1) the  
344 frequency and duration of bet hedging (persistence) in bacteria is heritable (Rotem et al., 2010),  
345 (2) different patterns of antibiotic treatment can select for a high frequency of bet hedgers (Van  
346 den Bergh et al., 2016), (3) antibiotic tolerance is determined by evolution of cell cycle reentry  
347 timing (lag times) (Fridman et al., 2014), and (4) lag times evolve as a function of the duration of  
348 antibiotic treatment (Fridman et al., 2014). Together with our results these findings link bet  
349 hedging strategies in microorganisms with the diversity of bet hedging strategies in higher  
350 eukaryotes, drawing parallels for example with the pioneering studies of seed dormancy bet  
351 hedging in desert annuals (Cohen, 1967). In microorganisms, when cautious cells respond to  
352 environmental stress with longer lag times whose frequency can be tuned/evolve to any value  
353 between 0 and 1, we suggest this be called “tunable bet hedging” to distinguish it from  
354 previously described pre-adaptive “stochastic bet hedging”.

355 In yeast as in multicellular organisms, fitness depends on reproduction in capricious and  
356 potentially lethal environments whose severity and duration are also unpredictable. Similar to  
357 seeds in dormancy, microorganisms in nature spend a large fraction of their time in post-diauxic  
358 or quiescent phases where they are naturally stress resistant but must mitigate risks when they  
359 resume growth or reproduction in potentially lethal environments (Gray et al., 2004). While

360 classical evolutionary models assign fitness directly to genotypes, mutations, and mean trait  
361 values without consideration of the genotype-to-phenotype map, molecular models provide  
362 detailed mechanisms of development but rarely consider the effects of natural genetic variation.  
363 Many studies of phenotypic diversity in yeast and bacteria are conducted in one or a few strains,  
364 but here we studied well-characterized osmotic stress signaling responses on a backdrop of  
365 natural variation in 50 yeast genotypes adapted to diverse ecologies. This enabled our  
366 identification of negative feedback controlling perfect adaptation and robust recovery of steady-  
367 state viability in exponential cultures experiencing moderate osmotic stress, and the combined  
368 strategies of predictive plasticity and diversified bet hedging in post diauxic cultures responding  
369 to more severe conditions. It is increasingly clear that labyrinthine developmental mechanisms –  
370 that are themselves controlled by genetic variation – translate genotypes into phenotypes with  
371 variable fidelity that can also be selected (Yvert et al., 2013). Evolution of the genotype-  
372 phenotype map across different environments enables the honing of predictive plasticity and  
373 selection on bi-stable states required for the evolution of bet hedging (Rotem et al., 2010;  
374 Rutherford, 2003).  
375

376 **Experimental procedures**

377

378 **Strain acquisition and deposition**

379 Over 200 unique wild and industrial diploid strains of *Saccharomyces cerevisiae* were obtained  
380 from the fungal diversity collection of Centraalbureau voor Schimmelcultures (CBS), an institute  
381 of the Royal Netherlands Academy of Arts and Sciences in Utrecht, Netherlands  
382 (<http://www.cbs.knaw.nl>). Strains that were modified for this report are listed in Tables 1 and  
383 Table 1–table supplement S1. They have been deposited to the Yeast Genetic Resources Lab  
384 of the National BioResource Project in Osaka, Japan  
385 ([http://yeast.lab.nig.ac.jp/nig/index\\_en.html/](http://yeast.lab.nig.ac.jp/nig/index_en.html/)).

386

387 **Haploid *MATa* library of wild and industrial genotypes**

388 Our goal was make a large library of haploid derivatives of wild and industrial strains in which to  
389 survey the effects of genetic variation at the level of osmotic stress signaling and downstream  
390 response. A total of 50 strains have been completely validated, and many others are in the  
391 pipeline. Ours is the largest such library of which we are aware and the results we report here  
392 show it should be generally useful – e.g. we have a large and representative sample of natural  
393 variation with bet hedgers ranging from almost completely cautious to completely reckless and  
394 sufficient ability to detect statistically significant effects. The first step in our library construction  
395 pipeline was to delete the *HO* locus of each strain by replacement with the KanMX4 marker  
396 gene and “barcodes” to permanently label each strain while preventing homothalasm (Table 1–  
397 table supplement S1)(Giaever et al., 2002; Shoemaker et al., 1996). The KanMX4 gene was  
398 PCR-amplified for this purpose with primers containing the barcode sequences(Wach et al.,  
399 1994). Next, kanamycin-resistant transformants were grown in pre-sporulation medium  
400 containing 10% glucose followed by sporulation under starvation conditions in 1% potassium  
401 acetate. Although the strains differ in their sporulation efficiency and optimal conditions (see  
402 strain information at <http://www.cbs.knaw.nl>), we found it was most efficient to put strains  
403 through repeated rounds of a general sporulation protocol rather than trying to optimize the  
404 conditions for each strain. The *MATa* haploids were identified by “schmoo” formation in 96-well  
405 plates containing alpha factor and confirmed by crossing to a G418-sensitive, clonNAT-resistant  
406 *MATalpha* tester strain and selection on double-antibiotic plates. Next we deleted the *URA3*  
407 gene using a standard gene deletion method and selected the *ura3Δ* clones by replica plating  
408 and selection on 5-FOA. Finally, *ho* and *ura3* deletions and the barcode sequences of each  
409 strain were verified by PCR and sequencing. Forty-nine wild strains and a laboratory strain  
410 meeting these criteria were used in this study (see Tables 1 and Table 1–table supplement S1  
411 for strain details).

412

413 **Synthetic population of *GPD1::GFP* wild/lab diploids**

414 The *MATalpha* laboratory strain BY4742 was transformed to create a stably integrated  
415 *GPD1::GFP* reporter (G01) using a deletion cassette containing a *URA3* marker for selection on  
416 SC-URA plates (Gietz and Woods, 2002; Wach et al., 1994). A synthetic “population” of diploids  
417 was created by mating each strain in the library of *MATa* haploids (50 strains) with *MATalpha*  
418 G01 by mixing on SC-URA plates for 2 hours followed by streaking onto selective SC-  
419 URA+G418 plates. The 50 resulting wild/lab diploid strains all have 50% of their genes and the  
420 *GPD1::GFP* reporter from strain G01 in the BY4742 laboratory strain background (Table 1).  
421 After mating, it was necessary to screen for triploids or tetraploids, which express higher levels  
422 of *GPD1::GFP* and have higher tolerance to osmotic stress. Overnight cultures of wild/lab yeast  
423 were diluted 50-fold into fresh YPD+G418 and grown for an additional 4 hours, fixed by 1:3  
424 dilution into cold ethanol and re-suspended in 20 ug/ml RNase A to digest ribonucleic acids.  
425 Digested cells were stained with 30 ug/ml propidium iodide to label DNA and ploidy was  
426 determined by flow cytometry (FACS Calibur; Becton Dickinson).

427

#### 428 **Exponential and post-diauxic cultures**

429 Fresh cultures were generated for each experiment by replicating frozen 96-well plates onto  
430 YPD+G418 agar followed by 4 days growth at 21° C. To obtain mid-exponential cultures, freshly  
431 patched cells were grown in 2 ml liquid YPD+G418 cultures at with rotation (72 rpm) at 21° C.  
432 for 2 days. Two microliters of these suspensions were diluted into 2 ml of liquid YPD+G418 and  
433 grown at 21° C. for 14 hours (e.g. 5 rounds of cell division on average, with strain ODs ranging  
434 from 0.80 – 1.44). For post-diauxic cultures, freshly patched cells were grown in 2 ml liquid  
435 YPD+G418 cultures at with rotation (72 rpm) at 21° C. for 4 days. Strains cultured up to 8-days  
436 post-diauxic growth were tested for osmotic stress resistance and we found that 4 day cultures  
437 were already maximally resistant (not shown).

438

#### 439 **Survival plating assays**

440 To determine the adaptation limit of each strain (Table 3), post-diauxic cultures were diluted to  
441 OD<sub>600</sub> of 0.1 with exhausted YPD (to prevent re-growth), sonicated for 5 seconds at a low  
442 setting (2.5; Sonifier Cell Disrupter, Model W185) and plated (5 ul) on 96-well YPD plates  
443 containing KCl ranging from 2.0 to 3.0 M. Growth was examined for up to 2 months at 21° C.  
444 Viability and static survival under osmotic stress (Figure 2B) was determined after incubation in  
445 96-well microtiter plates containing liquid media with increasing concentrations of KCl for the  
446 times indicated, followed by plating on iso-osmolar YPD agar plates.

447

#### 448 **Microfluidics**

449 We used custom made microfluidics devices with two fluid inputs as described (Bennett et al.,  
450 2008). When performing microfluidics with post-diauxic cells, post-diauxic cultures were  
451 inoculated into devices with exhausted YPD medium and allowed to stabilize for a few hours  
452 prior to osmotic stress. Experiments were run at ambient room temperature and observed using

453 a Nikon TS100 inverted microscope. Recordings were made using a Photometrics CoolSnap  
454 HQ2 digital camera operated by Metavue (Molecular Dynamics). Analysis of acquired images  
455 was performed using Image J software (<https://imagej.nih.gov/ij/>).

456

### 457 **Flow cytometry**

458 For flow cytometry, after osmotic stress treatments 4 ml of PBS was added to each culture.  
459 Cells were isolated by centrifugation and resuspended in 1 ml PBS, transferred to FACS tubes,  
460 sonicated (5 seconds at level 3, Sonifier Cell Disrupter, Model W185) and stained with 3 ug/ml  
461 propidium iodide (PI) to monitor viability. After 20 min GFP fluorescence and viability were  
462 quantified using a FACS Calibur flow cytometer (Becton Dickinson) that had been calibrated  
463 prior to each use with SPHERO Rainbow Fluorescent Particles, 3.0 – 3.4 um (BD Biosciences).  
464 Flow cytometry data were gated using magnetic windows in FlowJo software to eliminate cell  
465 fragments, clumped and dead (PI-positive) cells (<http://www.flowjo.com/>).

466 For analysis, raw data for the viable cells in each sample (forward scatter, side scatter and  
467 GFP fluorescence data; up to 10,000 cells/sample) were extracted into an SQL database. Cell  
468 data were scaled for linearity (e.g.  $FLH1^{1/3}$ ,  $FSC^{1/3}$ ,  $SSC^{1/2}$  for GFP fluorescence, forward  
469 scatter, and side scatter, respectively). Distributions of *GPD1::GFP* accumulation in exponential  
470 cultures were unimodal, and therefore well-defined using a single mean (e.g. Figure 1–figure  
471 supplement S1). By contrast, *GPD1::GFP* accumulations of cells in post-diauxic cultures were clearly  
472 multimodal at many time points (Figure 2–figure supplement 1). To identify different  
473 distributions of cells we used machine learning was performed using the sklearn.mixture option  
474 in the Gaussian Mixture Model (GMM) algorithm of the Python scikit package ([http://scikit-  
475 learn.org/](http://scikit-learn.org/)). The GMM algorithm identified parameters of the four most-likely Gaussian (defined  
476 by means and covariances) given the data for each sample. The 2-dimensional fits of  
477 *GPD1::GFP* and forward scatter data distinguished different cell types slightly better than fitting  
478 *GPD1::GFP* only; adding side scatter to fit distributions in 3-dimensional space little additional  
479 resolution. The number of Gaussians to be fit is a parameter that must be provided to the  
480 model. We used Bayesian information criteria (BIC) to determine that the data were well  
481 described by four distributions. In samples containing obviously fewer than four distributions, the  
482 under-populated distributions were assigned a correspondingly low frequency of cells.

483

### 484 **Clustering**

485 To group, and ultimately rank, the strains according to their osmotic stress signaling responses  
486 to 2.5 M KCl during post-diauxic growth we used hierarchical clustering with Wards method in  
487 the fastcluster Python implementation (<http://www.jstatsoft.org/v53/i09/>)<sup>34</sup>. First we created state  
488 vectors of each strains behavior. Cell distributions were binned onto a 100 X 100 2-D grid  
489 according to their *GPD1::GFP* and forward scatter data, smoothed with Python  
490 `scipyndimage.filters.gaussian_filter` and normalized to define a linear 10,000 element state  
491 vector for each sample (strain, time point). While 100 bins on each axis where sufficient to

492 capture detailed distributions while allowing efficient computation, we found stronger clustering  
493 when performing the same analysis using the combined *GPD1::GFP* and forward scattering  
494 data. The osmotic stress response up to 168 hours was defined by the vectors for each of the 7  
495 time points, successively appended to form a 70,000 element time-line vector representing the  
496 combined evolution of *GPD1::GFP* accumulation and forward scatter data.

497 The time-line vectors were used to compute a distance matrix between strains using the  
498 symmetric Kullback-Leibler divergence. As each strains and time point was replicated between  
499 4 and 15 times, we controlled for variation in sampling and clustering outcomes by randomly  
500 drawing samples for each strain and time point with equal probability. Clustering was repeated  
501 for a total of 17,000 permutations requiring 43 hours of computation time on a 3.7 GHz Intel  
502 7 iMac. This was sufficient to achieve stable Monte-Carlo statistics. Computational sorting of  
503 time-series distributions resolved 6 clades differentiated for rates of GFP accumulation,  
504 adaptation and survival. The fraction of permutations in which each strain grouped with more  
505 than half of the other strains in its mean cluster was used to rank that strain's behavior relative  
506 to the other strains in its group (clustering statistics; Table 5).

507

#### 508 **Author contributions**

509 YH designed and performed experiments, data analysis, figures and writing for initial versions of  
510 this manuscript. SB performed modeling, database construction, data analysis, statistical  
511 design, computer programming, writing and editorial support. WLP designed and trained us in  
512 microfluidics devices. SR conceptual design, workflow for wild strain collection, data analysis,  
513 model development, figures and writing.

514

#### 515 **Acknowledgments**

516 We thank Lisa Castenada, Tanya Gottlieb, Adrienne Hughes, Brandon (Tommy) Huynh, Katie  
517 Michaelsen, Rachel Rodman, and numerous undergraduate helpers for construction and  
518 validation of the wild strain collection, Jeff Hasty for advice on microfluidics and Stéphane  
519 Douady and Pierre-Yves Bourguignon for discussions and advice on scaling and clustering.  
520 This research was supported by a Scholar Award from the Damon Runyon Cancer Research  
521 Foundation (SR) and the Lady Tata Memorial Trust (YH).

#### 522 **References**

523 Arnoldini, M., Mostowy, R., Bonhoeffer, S., and Ackermann, M. (2012). Evolution of Stress  
524 Response in the Face of Unreliable Environmental Signals. *PLoS Comput. Biol.* 8.  
525 Babazadeh, R., Furukawa, T., Hohmann, S., and Furukawa, K. (2014). Rewiring yeast  
526 osmostress signalling through the MAPK network reveals essential and non-essential roles of  
527 Hog1 in osmoadaptation. *Sci. Rep.* 4, 4697.  
528 Bennett, M.R., Pang, W.L., Ostroff, N.A., Baumgartner, B.L., Nayak, S., Tsimring, L.S., and  
529 Hasty, J. (2008). Metabolic gene regulation in a dynamically changing environment. *Nature* 454,  
530 1119–1122.  
531 Van den Bergh, B., Michiels, J.E., Wenseleers, T., Windels, E.M., Vanden Boer, P., Kestemont,

532 D., De Meester, L., Verstrepen, K.J., Verstraeten, N., Fauvart, M., et al. (2016). Frequency of  
533 antibiotic application drives rapid evolutionary adaptation of *Escherichia coli* persistence. *Nat.*  
534 *Microbiol.* *1*, 16020.

535 Boy-Marcotte, E., Perrot, M., Bussereau, F., Boucherie, H., and Jacquet, M. (1998). Msn2p and  
536 Msn4p control a large number of genes induced at the diauxic transition which are repressed by  
537 cyclic AMP in *Saccharomyces cerevisiae*. *J. Bacteriol.* *180*, 1044–1052.

538 Brachmann, C.B., Davies, A., Cost, G.J., Caputo, E., Li, J., Hieter, P., and Boeke, J.D. (1998).  
539 Designer deletion strains derived from *Saccharomyces cerevisiae* S288C: A useful set of strains  
540 and plasmids for PCR-mediated gene disruption and other applications. *Yeast* *14*, 115–132.

541 Clotet, J., and Posas, F. (2007). Control of Cell Cycle in Response to Osmostress: Lessons  
542 from Yeast (Elsevier Masson SAS).

543 Cohen, D. (1967). Optimizing reproduction in a randomly varying environment when a  
544 correlation may exist between the conditions at the time a choice has to be made and the  
545 subsequent outcome. *J. Theor. Biol.* *16*, 1–14.

546 Donaldson-Matasci, M.C., Bergstrom, C.T., and Lachmann, M. (2013). When unreliable cues  
547 are good enough. *Am. Nat.* *182*, 313–327.

548 Feder, M.E., and Hoffmann, G.E. (1999). Heat-shock proteins , molecular chaperones , and the  
549 stress response□: evolutionary and ecological ecology.

550 Fridman, O., Goldberg, A., Ronin, I., Shoshitashvili, N., and Balaban, N.Q. (2014). Optimization of lag  
551 time underlies antibiotic tolerance in evolved bacterial populations. *Nature* *513*, 418–421.

552 Galdieri, L., Mehrotra, S., Yu, S., and Vancura, A. (2010). Transcriptional Regulation in Yeast  
553 during Diauxic Shift and Stationary Phase. *Omi. A J. Integr. Biol.* *14*, 629–638.

554 Giaever, G., Chu, A.M., Ni, L., Connelly, C., Riles, L., Véronneau, S., Dow, S., Lucau-Danila, A.,  
555 Anderson, K., André, B., et al. (2002). Functional profiling of the *Saccharomyces cerevisiae*  
556 genome. *Nature* *418*, 387–391.

557 Gietz, R.D., and Woods, R. a. (2002). Transformation of yeast by lithium acetate/single-  
558 stranded carrier DNA/polyethylene glycol method. *Methods Enzymol.* *350*, 87–96.

559 Gray, J. V, Petsko, G. a, Johnston, G.C., Ringe, D., Singer, R. a, and Werner-Washburne, M.  
560 (2004). “Sleeping beauty”: quiescence in *Saccharomyces cerevisiae*. *Microbiol. Mol. Biol. Rev.*  
561 *68*, 187–206.

562 Hohmann, S. (2002). Osmotic Stress Signaling and Osmoadaptation in Yeasts. *Microbiol. Mol.*  
563 *Biol. Rev.* *66*, 300–372.

564 Hohmann, S., Krantz, M., and Nordlander, B. (2007). Yeast Osmoregulation (Elsevier Masson  
565 SAS).

566 Jacoby, T., Flanagan, H., Faykin, A., Seto, A.G., Mattison, C., and Ota, I. (1997). Two Protein-  
567 tyrosine Phosphatases Inactivate the Osmotic Stress Response Pathway in Yeast by Targeting  
568 the Mitogen-activated Protein Kinase, Hog1. *J. Biol. Chem.* *272*, 17749–17755.

569 De Jong, I.G., Haccou, P., and Kuipers, O.P. (2011). Bet hedging or not? A guide to proper  
570 classification of microbial survival strategies. *BioEssays* *33*, 215–223.

571 King, O.D., and Masel, J. (2007). The evolution of bet-hedging adaptations to rare scenarios.  
572 *Theor. Popul. Biol.* *72*, 560–575.

573 Kirschner, M., and Gerhart, J. (1998). Evolvability. *Proc. Natl. Acad. Sci. U. S. A.* *95*, 8420–  
574 8427.

575 Lee, Y.J., Jeschke, G.R., Roelants, F.M., Thorner, J., and Turk, B.E. (2012). Reciprocal  
576 Phosphorylation of Yeast Glycerol-3-Phosphate Dehydrogenases in Adaptation to Distinct  
577 Types of Stress. *Mol. Cell. Biol.* *32*, 4705–4717.

578 Levy, S.F., Ziv, N., and Siegal, M.L. (2012). Bet hedging in yeast by heterogeneous, age-  
579 correlated expression of a stress protectant. *PLoS Biol.* *10*.

580 Meyers, L.A., and Bull, J.J. (2002). Fighting change with change: Adaptive variation in an  
581 uncertain world. *Trends Ecol. Evol.* *17*, 551–557.

582 Miermont, A., Waharte, F., Hu, S., McClean, M.N., Bottani, S., Léon, S., and Hersen, P. (2013).

583 Severe osmotic compression triggers a slowdown of intracellular signaling, which can be  
584 explained by molecular crowding. *Proc. Natl. Acad. Sci. U. S. A.* *110*, 5725–5730.  
585 Mortimer, R.K., and Johnston, J.R. (1986). Genealogy of principal strains of the yeast genetic  
586 stock center. *Genetics* *113*, 35–43.  
587 Muzzey, D., Gómez-Urbe, C. a., Mettetal, J.T., and van Oudenaarden, A. (2009). A Systems-  
588 Level Analysis of Perfect Adaptation in Yeast Osmoregulation. *Cell* *138*, 160–171.  
589 Nadal, E. de, Alepuz, P., and Posas, F. (2002). Dealing with osmostress through MAP kinase  
590 activation. *EMBO Rep.* *3*, 735–740.  
591 Philippi, T., and Seger, J. (1989). Hedging one's evolutionary bets, revisited. *Trends Ecol. Evol.*  
592 (Personal Ed. *4*, 41–44.  
593 Ratcliff, W.C., and Denison, R.F. (2010). Individual-Level Bet Hedging in the Bacterium  
594 *Sinorhizobium meliloti*. *Curr. Biol.* *20*, 1740–1744.  
595 Ratcliff, W.C., Hawthorne, P., and Libby, E. (2014). Courting disaster: How diversification rate  
596 affects fitness under risk. *Evolution* 1–10.  
597 Remize, F., Barnavon, L., and Dequin, S. (2001). Glycerol export and glycerol-3-phosphate  
598 dehydrogenase, but not glycerol phosphatase, are rate limiting for glycerol production in  
599 *Saccharomyces cerevisiae*. *Metab. Eng.* *3*, 301–312.  
600 Richter, K., Haslbeck, M., and Buchner, J. (2010). The Heat Shock Response: Life on the Verge  
601 of Death. *Mol. Cell* *40*, 253–266.  
602 Rotem, E., Loinger, A., Ronin, I., Levin-Reisman, I., Gabay, C., Shores, N., Biham, O., and  
603 Balaban, N.Q. (2010). Regulation of phenotypic variability by a threshold-based mechanism  
604 underlies bacterial persistence. *Proc. Natl. Acad. Sci. U. S. A.* *107*, 12541–12546.  
605 Rutherford, S.L. (2000). From genotype to phenotype: buffering mechanisms and the storage of  
606 genetic information. *Bioessays* *22*, 1095–1105.  
607 Rutherford, S.L. (2003). Between genotype and phenotype: protein chaperones and evolvability.  
608 *Nat. Rev. Genet.* *4*, 263–274.  
609 Saito, H., and Posas, F. (2012). Response to hyperosmotic stress. *Genetics* *192*, 289–318.  
610 Shoemaker, D.D., Lashkari, D. a, Morris, D., Mittmann, M., and Davis, R.W. (1996). Quantitative  
611 phenotypic analysis of yeast deletion mutants using a highly parallel molecular bar-coding  
612 strategy. *Nat. Genet.* *14*, 450–456.  
613 Simons, A.M. (2011). Modes of response to environmental change and the elusive empirical  
614 evidence for bet hedging. *Proc. Biol. Sci.* *278*, 1601–1609.  
615 Tomanek, L. (2010). Variation in the heat shock response and its implication for predicting the  
616 effect of global climate change on species' biogeographical distribution ranges and metabolic  
617 costs. *J. Exp. Biol.* *213*, 971–979.  
618 Wach, A., Brachat, A., Pöhlmann, R., and Philippsen, P. (1994). New heterologous modules for  
619 classical or PCR-based gene disruptions in *Saccharomyces cerevisiae*. *Yeast* *10*, 1793–1808.  
620 West-Eberhard, M.J. (2003). Developmental plasticity and evolution.  
621 Wurgler-Murphy, S.M., Maeda, T., Witten, E. a, and Saito, H. (1997). Regulation of the  
622 *Saccharomyces cerevisiae* HOG1 mitogen-activated protein kinase by the PTP2 and PTP3  
623 protein tyrosine phosphatases. *Mol. Cell. Biol.* *17*, 1289–1297.  
624 Yi, T.M., Huang, Y., Simon, M.I., and Doyle, J. (2000). Robust perfect adaptation in bacterial  
625 chemotaxis through integral feedback control. *Proc. Natl. Acad. Sci. U. S. A.* *97*, 4649–4653.  
626 Yvert, G., Ohnuki, S., Nogami, S., Imanaga, Y., Fehrmann, S., Schacherer, J., and Ohya, Y.  
627 (2013). Single-cell phenomics reveals intra-species variation of phenotypic noise in yeast. *BMC*  
628 *Syst. Biol.* *7*, 54.  
629

630 **Tables**

631 **Table 1. Strains and aliases used in this study.** See Table 1–table supplement S1 for details  
 632 about each of the 49 wild haploid strain derivatives (WHXXX). For brevity, figures are labeled  
 633 with the wild parent strain number (WXXX; see Table S1 for details).

634

Strain	Genotype	Source
WHXXX	<i>MATa ura3Δ0 hoΔ::barcode::KanMX4</i>	Haploid <i>MATa</i> isolates of wild strains. This study; see Table S1 for details.
BY41	<i>MATa his3D1 leu2Δ0 met15Δ0 ura3Δ0 flo8-1 hoΔ::barcode::KanMX4</i>	Barcoded, <i>MATa</i> derivative of BY4742 used as a control genotype for the laboratory strain background. This study.
BY4742 (BY01)	<i>MATalpha his3D1 leu2Δ0 lys2Δ0 ura3Δ0 flo8-1</i>	<i>MATalpha</i> laboratory strain. BY4741 and BY4742 backgrounds derive from a wild diploid isolated in Merced, California in 1938 on figs (EM93(Mortimer and Johnston, 1986); S228C(Brachmann et al., 1998)). They are distinguished primarily by the many generations it has been under laboratory selection.
G01	<i>MATalpha his3D1 leu2Δ0 lys2Δ0 ura3Δ0 flo8-1 gpd1D::GFP::URA3</i>	Used for monitoring GPD1. BY4742 background; this study.
WXXX.BY16	<i>MATa/MATalpha LYS2/lys2Δ0 ura3Δ0/URA3 FLO8/flo8-1 hoΔ::barcode::KanMX4/ho</i>	Controls. A set of 49 wild/lab plus 1 BY41.BY16 control for effect of marker gene deletions. This study; see Table S1 for details.
WXXX.G01	<i>MATa/MATalpha HIS3/his3D1 LEU2/leu2Δ0 LYS2/lys2Δ0 ura3Δ0/ura3Δ0 FLO8/flo8-1 hoΔ::barcode::KanMX4/ho GPD1/gpd1D::GFP::URA3</i>	Synthetic population of wild/lab diploids for GPD1 quantification. This study; see Table S1 for details.

635

636

637 **Table 1– table supplement S1. Haploid derivatives of wild strains.**

638 The source for all wild strains in this study was the strain collection of the Royal Netherlands  
639 Academy of Arts and Sciences over the past 100 years (Table 1 and Table S1). All strains used  
640 in this study have been deposited to the Yeast Genetic Resources Lab of the National  
641 BioResource Project in Osaka, Japan [http://yeast.lab.nig.ac.jp/nig/index\\_en.html](http://yeast.lab.nig.ac.jp/nig/index_en.html) .  
642

**Table1 S1. Haploid derivatives of wild strains.**

Alias	MAT	Genotype	Comments
WH027	a	MATa ura3Δ0 hoΔ::barcode::KanMX4	Original CBS #: CBS 459; isolated in 1938 in Castellina, Italy from grape must; barcode #29(Uptag sequence:GGCCCGCACACAATTAGGAA, Downtag sequence:GCGCCGCATTAACCTAACTA)
WH030	a	MATa ura3Δ0 hoΔ::barcode::KanMX4	Original CBS #: CBS 1508; isolated in 1927 from starter for sorghum brandy; YH note: mating defective, hard to make wild/lab diploids; barcode #16(Uptag sequence:GTCCGAACTATCAACACGTA, Downtag sequence:GCGCACGAGAAACCTCTTAA)
WH033	a	MATa ura3Δ0 hoΔ::barcode::KanMX4	Original CBS #: CBS 405 ; isolated in 1925 in West Africa from catabo for billi wine, from Osbeckia grandiflora; barcode #187(Uptag sequence:CCGTGTAATGCAATTACGATC, Downtag sequence:CCATCTTTGGTAATGTGAGG)
WH035	a	MATa ura3Δ0 hoΔ::barcode::KanMX4	Original CBS #: CBS 5822; isolated in 1967 from malt wine; barcode #30(Uptag sequence:GGTCTATGCAAACACCCGAA, Downtag sequence:GCCGTCTTGACAACCTTATA)
WH037	a	MATa ura3Δ0 hoΔ::barcode::KanMX4	Original CBS #: CBS 1395; isolated in 1922 from an unknown source ; barcode #235(Uptag sequence:GGCTAAGGGACAACACCTCA, Downtag sequence:GCCCGGCACATAGAAGTAAC)

WH041	a	MATa ura3 $\Delta$ 0 ho $\Delta$ ::barcode::KanMX4	Original CBS #: CBS 5635; isolated in 1958 in South Africa from grape must; barcode #2(Uptag sequence:CCATGATGTAAACGATCCGA, Downtag sequence:TATATGGCAGCAGATCGCCG)
WH042	a	MATa ura3 $\Delta$ 0 ho $\Delta$ ::barcode::KanMX4	Original CBS #: CBS 3081; isolated in 1958 in Spain from alpechin; barcode #12(Uptag sequence:GTGCGAACCAACGTACTACA, Downtag sequence:GCAGGAACACCACAGGGTTA)
WH044	a	MATa ura3 $\Delta$ 0 ho $\Delta$ ::barcode::KanMX4	Original CBS #: CBS 422; isolated in 1926 in Odessa, Ukraine from beer; barcode #135(Uptag sequence:CCCGCGATTGTAATGAATAG, Downtag sequence:CATACTACGTGGGACAGTTG)
WH050	a	MATa ura3 $\Delta$ 0 ho $\Delta$ ::barcode::KanMX4	Original CBS #: CBS 5112; isolated in 1962 in Spain from grape must; barcode #49(Uptag sequence:CTTACTGATAGCGTAGAGGT, Downtag sequence:GTGGTCTGCAAACCCAACAA)
WH134	a	MATa ura3 $\Delta$ 0 ho $\Delta$ ::barcode::KanMX4	Original CBS #: CBS 2964; isolated in 1947 in Copenhagen, Denmark from distiller's rum yeast; barcode #18(Uptag sequence:GCCCTGATAACAAGGTGTAA, Downtag sequence:GCGCCTATTACACAAACGTA)
WH136	a	MATa ura3 $\Delta$ 0 ho $\Delta$ ::barcode::KanMX4	Original CBS #: CBS 2811; isolated in 1957 from wine; wine yeast; barcode #20(Uptag sequence:GTGAGCGAAACACCGCGTAA, Downtag sequence:GGTAATACGCAACTCCTCTA)
WH150	a	MATa ura3 $\Delta$ 0 ho $\Delta$ ::barcode::KanMX4	Original CBS #: CBS 2962; isolated in 1947 in Copenhagen, Denmark from ; distiller's rum yeast; barcode #15(Uptag sequence:GCCGTAGCCACAAGAGTTAA, Downtag sequence:GCGGCCACTTACACAAATTA)

WH153	a	MATa ura3 $\Delta$ 0 ho $\Delta$ ::barcode::KanMX4	Original CBS #: CBS 6458; isolated in 1972 location not reported; barcode #37(Uptag sequence:GGGACCGCCAAAGCTATCAA, Downtag sequence:GTGAACAATAACGGCCTTGA)
WH157	a	MATa ura3 $\Delta$ 0 ho $\Delta$ ::barcode::KanMX4	Original CBS #: CBS 6506; isolated in 1973 in UK brewery; killer yeast; barcode #53(Uptag sequence:CTGAGCGTAGGATATTCCGT, Downtag sequence:GCCGGTCGCAAACACTATAAA)
WH163	a	MATa ura3 $\Delta$ 0 ho $\Delta$ ::barcode::KanMX4	Original CBS #: CBS 6914; isolated in 1977 in Spain from white wine; barcode #51(Uptag sequence:CTACGTCGGCTCATAGTCGT, Downtag sequence:GCTCTCGGCCAAGGAAACAA)
WH164	a	MATa ura3 $\Delta$ 0 ho $\Delta$ ::barcode::KanMX4	Original CBS #: CBS 6978; isolated in 1984 from wine; wine yeast; barcode #59(Uptag sequence:CACTCGGATTCAGTTCTAGT, Downtag sequence:GGCCTTGCCAAACAGTCAAA)
WH166	a	MATa ura3 $\Delta$ 0 ho $\Delta$ ::barcode::KanMX4	Original CBS #: CBS 7072; isolated in 1980 from distillate; barcode #62(Uptag sequence:CCTAGTTCGAGATTGCGAGT, Downtag sequence:GTGGTCGCCCAAGCAACAAA)
WH167	a	MATa ura3 $\Delta$ 0 ho $\Delta$ ::barcode::KanMX4	Original CBS #: CBS 7173; isolated in 1985 from catabo for billi wine; wine yeast; barcode #43(Uptag sequence:CAGTATGCTAGATTCCGGGT, Downtag sequence:GTCCTCGCAAGAAAGGCCAA)
WH173	a	MATa ura3 $\Delta$ 0 ho $\Delta$ ::barcode::KanMX4	Original CBS #: CBS 8615; isolated in 1998 in Italy from grape must; dry yeast for wine making; barcode #61(Uptag sequence:CCTGTAGTACGAGTATGAGT, Downtag sequence:GGTCTGCCCAAGTCACAAA)

WH178	a	MATa ura3 $\Delta$ 0 ho $\Delta$ ::barcode::KanMX4	Original CBS #: CBS 1192; isolated in 1928 from wine; wine yeast; barcode #155(Uptag sequence:CGCACACGATTAAGGTCCAG, Downtag sequence:CACTGTTGGTAAGGTCTATG)
WH179	a	MATa ura3 $\Delta$ 0 ho $\Delta$ ::barcode::KanMX4	Original CBS #: CBS 1193; isolated in 1928 from wine; wine yeast; barcode #70(Uptag sequence:CAATAGGGTGTGACAGTTCT, Downtag sequence:CTACTTCGCGTGAGCTGGTT)
WH189	a	MATa ura3 $\Delta$ 0 ho $\Delta$ ::barcode::KanMX4	Original CBS #: CBS 1241; isolated in 1930 from an unknown source ; barcode #212(Uptag sequence:CCACTTAGTTCAATAGGCCG, Downtag sequence:CCGAGTATTACATTCTCACC)
WH195	a	MATa ura3 $\Delta$ 0 ho $\Delta$ ::barcode::KanMX4	Original CBS #: CBS 1256; isolated in 1937 from port wine; barcode #123(Uptag sequence:CGTGGAGCAGTTCGTATAAT, Downtag sequence:CTCGACGCTGGACGTTATGT)
WH202	a	MATa ura3 $\Delta$ 0 ho $\Delta$ ::barcode::KanMX4	Original CBS #: CBS 7372; isolated in 1988; killer yeast, K2Rd (Young & Yagiu), K2R2 (Wickner); barcode #119(Uptag sequence:CAACGTAGAGTGAGGTACAT, Downtag sequence:CACTTAGCTTAGACTCGTGT)
WH203	a	MATa ura3 $\Delta$ 0 ho $\Delta$ ::barcode::KanMX4	Original CBS #: CBS 7438; isolated in 1989 from wine; wine yeast; barcode #65(Uptag sequence:CTTTCGGACGTATGTGCAGT, Downtag sequence:CCTTGATGATAGAGGGCTTT)
WH206	a	MATa ura3 $\Delta$ 0 ho $\Delta$ ::barcode::KanMX4	Original CBS #: CBS 7833; isolated in 1994 in Missouri, USA from lung of a man with immune deficiency syndrome; virulent strain; barcode #82(Uptag sequence:CATACAAAGAGAGGTGCCT, Downtag sequence:CCCTTGCGATTGGTGACGTT)

WH211	a	MATa ura3Δ0 hoΔ::barcode::KanMX4	Original CBS #: CBS 7838; isolated in 1994 in USA from patient; barcode #144(Uptag sequence:CGATACAAGTAAGTTGCGAG, Downtag sequence:CCTCTTACGAGATAGCGGTG)
WH215	a	MATa ura3Δ0 hoΔ::barcode::KanMX4	Original CBS #: CBS 7962; isolated in 1984 in Sao Paulo, Brazil from fermenting concentrated syrup from sugar cane; barcode #94(Uptag sequence:CCCGATTGAGGCATGGTTAT, Downtag sequence:CGCTTCGAGTATGGGATATT)
WH217	a	MATa ura3Δ0 hoΔ::barcode::KanMX4	Original CBS #: CBS 7964; isolated in 1995 in Sao Paulo, Brazil from fermenting concentrated syrup from sugar cane; barcode #92(Uptag sequence:CGCGGAGTATAGAGCTTTAT, Downtag sequence:CAATCGCTCGGAGGCGTATT)
WH219	a	MATa ura3Δ0 hoΔ::barcode::KanMX4	Original CBS #: CBS 439 ; isolated in 1933 in Lager Schartel, Germany from Silvaner grapes; barcode #93(Uptag sequence:CGACCCTGATGATCCTTTAT, Downtag sequence:CTACGGGCTCGATGCCTATT)
WH235	a	MATa ura3Δ0 hoΔ::barcode::KanMX4	Original CBS #: CBS 5952; isolated in 1968; barcode #102(Uptag sequence:GGCTACGATACATCTTCATC, Downtag sequence:CATTTGTAACCAGTTCGCTC)
WH238	a	MATa ura3Δ0 hoΔ::barcode::KanMX4	Original CBS #: CBS 6223; isolated in 1969 in Chile from grape juice; radiation resistant; barcode #104(Uptag sequence:CTATGTGCGGTAAGACGTAT, Downtag sequence:CGGCGTAGATTGTTAGCATT)
WH242	a	MATa ura3Δ0 hoΔ::barcode::KanMX4	Original CBS #: CBS 6333; isolated in 1942 in Costa Rica from rotting banana; Strain name NRRL Y-1350 (synonymous designation; NRRL YB-210, NRRL-210, NRRL-B210; Mortimer and Johnston (1986), Genetics 113: 35); barcode #56(Uptag sequence:CCTGTAGATTGACGTGTAGT, Downtag sequence:GCCCTCGTGACAAATCGAAA)

WH244	a	MATa ura3 $\Delta$ 0 ho $\Delta$ ::barcode::KanMX4	Original CBS #: CBS 8266; isolated in 1996 in from rotting fig; Strain name X2180, derived from S288C by self-diploidization (Mortimer and Johnston (1986), Genetics 113: 35). Did not survive freeze-drying.; barcode #122(Uptag sequence:CAGAGGGCACTGTTCTTAAT, Downtag sequence:CCCTGCTGTAGAGGTTATGT)
WH245	a	MATa ura3 $\Delta$ 0 ho $\Delta$ ::barcode::KanMX4	Original CBS #: CBS 3000; isolated in 1956 in Pakistan from palm wine; wine yeast; barcode #138(Uptag sequence:CACATCGTTTAACTGGAG, Downtag sequence:CTAGGAGGTTACAGTCATTG)
WH248	a	MATa ura3 $\Delta$ 0 ho $\Delta$ ::barcode::KanMX4	Original CBS #: CBS 8049; isolated in 1981 from fish food; feed for fish and crustaceans; barcode #108(Uptag sequence:CGACCCGATGTAGTAGATAT, Downtag sequence:CCGCCGATGTGATATAATT)
WH249	a	MATa ura3 $\Delta$ 0 ho $\Delta$ ::barcode::KanMX4	Original CBS #: CBS 6069; isolated in 1981; hybrid strain (Y55-2 x JJ101); barcode #87(Uptag sequence:CACTGTGACCGAGGGATACT, Downtag sequence:CGCGCTATTATACTCGACTT)
WH255	a	MATa ura3 $\Delta$ 0 ho $\Delta$ ::barcode::KanMX4	Original CBS #: CBS 3090; isolated in 1958 from white grape must; barcode #72(Uptag sequence:CACTGTGGACGATACGGTCT, Downtag sequence:CTGTACGTGCGATACTCGTT)
WH276	a	MATa ura3 $\Delta$ 0 ho $\Delta$ ::barcode::KanMX4	Original CBS #: CBS 1394; isolated in 1924 from pressed yeast; distillery yeast; barcode #176(Uptag sequence:CCACCGATGTAATTTGAGTC, Downtag sequence:CACTCTGCGTTAATGTTGGG)
WH282	a	MATa ura3 $\Delta$ 0 ho $\Delta$ ::barcode::KanMX4	Original CBS #: CBS 1460; isolated in 1927 in Indonesia from fermenting fruit; barcode #115(Uptag sequence:CATACTTAGGGATCAGGGAT, Downtag sequence:CCTTGTCTGAGAGCCGTTGT)

WH285	a	MATa ura3 $\Delta$ 0 ho $\Delta$ ::barcode::KanMX4	Original CBS #: CBS 1479; isolated in 1928 from wine; wine yeast; barcode #240(Uptag sequence:GCGGCCAATAGTAAACTTCA, Downtag sequence:GCCGCCGTGATAAGAAACAC)
WH291	a	MATa ura3 $\Delta$ 0 ho $\Delta$ ::barcode::KanMX4	Original CBS #: CBS 1576; isolated in 1931 in Sulawesi, Indonesia from sap of Arenga palm; barcode #117(Uptag sequence:CCTGAGGACTTATTCACGAT, Downtag sequence:CATTGGATTAGACCGTGTGT)
WH292	a	MATa ura3 $\Delta$ 0 ho $\Delta$ ::barcode::KanMX4	Original CBS #: CBS 1582; isolated in 1948 in Portugal from wine; barcode #118(Uptag sequence:CCGATTAGAGGTTGACAGAT, Downtag sequence:CACTGACTTCGAGGTCGTGT)
WH294	a	MATa ura3 $\Delta$ 0 ho $\Delta$ ::barcode::KanMX4	Original CBS #: CBS 1585; isolated in 1934 from sake-moto; sake yeast; barcode #180(Uptag sequence:CATTAAGGCGCAGCTTTATC, Downtag sequence:CTATCCTAGAGATTTGAGGG)
WH301	a	MATa ura3 $\Delta$ 0 ho $\Delta$ ::barcode::KanMX4	Original CBS #: CBS 1594; isolated in 1936 from juice of aren palm; barcode #182(Uptag sequence:CACGTTTGCGAATAGGTATC, Downtag sequence:CAGATACTATTAAGTGCCGG)
WH340	a	MATa ura3 $\Delta$ 0 ho $\Delta$ ::barcode::KanMX4	Original CBS #: CBS 2805; isolated in 1954 from wine; wine yeast, particularly suitable for fruit wines; barcode #233(Uptag sequence:GCCGGGCTTAAATTGAATCA, Downtag sequence:GCTCCGACTGAAGAACTAAC)
WH343	a	MATa ura3 $\Delta$ 0 ho $\Delta$ ::barcode::KanMX4	Original CBS #: CBS 2808; isolated in 1954 from grapes (Blauer Portugieser); wine yeast, suitable for fruit wines, yields more than 18% of alcohol; barcode #224(Uptag sequence:CCCGTGAATATAAGTGAAGC, Downtag sequence:CCTGGATTTGAAGCGTATAG)

WH454	a	MATa ura3 $\Delta$ 0 ho $\Delta$ ::barcode::KanMX4	Original CBS #: CBS 6412; isolated in 1952 from sake; sake yeast; barcode #192(Uptag sequence:CCTTAGGGATAATGAGTTGC, Downtag sequence:CCAGTGTTCTAACGTGCAGG)
WH455	a	MATa ura3 $\Delta$ 0 ho $\Delta$ ::barcode::KanMX4	Original CBS #: CBS 440 ; isolated in 1934 in Taiwan from molasses; barcode #249(Uptag sequence:GCCCAGGCTAAATGTTAAGA, Downtag sequence:GAAGTACGCTCAAGACCGAC)
BC4741 (BY41)	a	MATa his3D1 leu2 $\Delta$ 0 met15 $\Delta$ 0 ura3 $\Delta$ 0 flo8-1 ho $\Delta$ ::barcode::KanMX4	Original CBS #: Lab strain, BY4741; isolated in 1938 in Merced, CA, USA from Rotting fig; BY4741 is derived from S288C, of which strain 88% of the gene pool is contributed by strain EM93 (Mortimer and Johnston (1986), Genetics 113: 35). Barcode #266(Uptag sequence:GGCCTAACTCAACAGACGGA, Downtag sequence:GCGCTCGACTAAGAGAAACC)

643

644

645

646 **Table 2. Negative feedback between rates of change in mean *GPD1::GFP* accumulation**  
 647 **and viability among strains.** Correlations confirm causality between rates of change in  
 648 *GPD1::GFP* accumulation and viability within (upper 3 rows) and between 2 hour time intervals  
 649 (below). Changes occurring in earlier intervals are listed first. To control for potential deviations  
 650 from normality, both parametric (Pearson's) and non-parametric (Spearman's) pairwise  
 651 correlations are shown. As in Figure 1 all 50 strains were tested at 0, 2, and 4 hours and 18  
 652 strains were tested at 6 hours (mean values represent a minimum of 3 replicates per strain).  
 653 Significant comparisons are in bold (JMP statistical software, SAS Institute; Cary, NC).

N	Variable	Interval (hrs)	Variable	Interval (hrs)	Pearson's r	Spearman's r	Prob> r	
							Pearson's	Spearman's
50	$\Delta$ GPD1::GFP	0 – 2	$\Delta$ viability	0 – 2	0.8235	0.7725	<b>&lt;.0001</b>	<b>&lt;.0001</b>
50	$\Delta$ GPD1::GFP	2 – 4	$\Delta$ viability	2 – 4	0.7739	0.7217	<b>&lt;.0001</b>	<b>&lt;.0001</b>
18	$\Delta$ GPD1::GFP	4 – 6	$\Delta$ viability	4 – 6	-0.2354	-0.1992	0.3470	0.4282
50	$\Delta$ viability	0 – 2	$\Delta$ GPD1::GFP	2 – 4	-0.7867	-0.7411	<b>&lt;.0001</b>	<b>&lt;.0001</b>
50	$\Delta$ viability	0 – 2	$\Delta$ viability	2 – 4	-0.9670	-0.9503	<b>&lt;.0001</b>	<b>&lt;.0001</b>
50	$\Delta$ GPD1::GFP	0 – 2	$\Delta$ GPD1::GFP	2 – 4	-0.7685	-0.7697	<b>&lt;.0001</b>	<b>&lt;.0001</b>
50	$\Delta$ GPD1::GFP	0 – 2	$\Delta$ viability	2 – 4	-0.8082	-0.7696	<b>&lt;.0001</b>	<b>&lt;.0001</b>
18	$\Delta$ viability	0 – 2	$\Delta$ viability	4 – 6	-0.1407	-0.2178	0.5777	0.3854
18	$\Delta$ viability	0 – 2	$\Delta$ GPD1::GFP	4 – 6	-0.3704	-0.2549	0.1303	0.3073
18	$\Delta$ GPD1::GFP	0 – 2	$\Delta$ viability	4 – 6	-0.0456	-0.0464	0.8573	0.8548
18	$\Delta$ GPD1::GFP	0 – 2	$\Delta$ GPD1::GFP	4 – 6	-0.4319	-0.4572	0.0735	0.0565
18	$\Delta$ viability	2 – 4	$\Delta$ viability	4 – 6	-0.0100	0.0733	0.9685	0.7726
18	$\Delta$ viability	2 – 4	$\Delta$ GPD1::GFP	4 – 6	0.4316	0.3333	0.0737	0.1765
18	$\Delta$ GPD1::GFP	2 – 4	$\Delta$ viability	4 – 6	0.1400	0.1207	0.5796	0.6332
18	$\Delta$ GPD1::GFP	2 – 4	$\Delta$ GPD1::GFP	4 – 6	0.3731	0.3602	0.1273	0.1421

654

655 **Table 3. Growth of post-diauxic cells at unprecedented limits of adaptation.** Shown are  
656 concentrations of agar media on which post-diauxic strains could grow and form colonies.

657

<b>[KCl] M</b>	<b>Wild/lab (<i>GPD1</i>) diploids*</b>
2.0	W455
2.6	W027, W035, W167, W202, W203, W242, W285, W454
2.7	W033, W041, W042, W134, W136, W150, W166, W178, W195, W215, W217, W219, W235, W248, W282, W291, W292, W294, BY41
2.8	W037, W044, W050, W153, W157, W163, W164, W179, W189, W206, W238, W244, W245, W249, W255, W276, W301, W340
2.9	W173, W211, W343

658

659

660 **Table 4. Osmotic stress signaling behavior (rank) predicted early and late viability of**  
 661 **post-diauxic cultures in osmotic stress.** Least squares predictions of early and late viability  
 662 by linear and 2<sup>nd</sup> order quadratic fits of fluorescence pre-accumulated into the G3 Gaussian at  
 663 time 0 (G3\_0) and ranked signaling behavior of 50 strains. The Bonferroni cutoff at the 0.05  
 664 level, based on 4 tests per data set, was 0.0125 (JMP statistical software, SAS Institute; Cary,  
 665 NC). Significant fits with lowest root mean squared errors and highest fraction of variation  
 666 explained ( $R^2$ ) shown in bold, predicted values for optimum (x) and value at optimum (y) for non-  
 667 significant fits are shown for comparison.  
 668

	G <sub>3</sub> fluorescence (AU) at time 0		Signaling (rank)	
	quadratic	linear	quadratic	linear
<b>0 hours, 0M KCl</b>				
probability > F	<b>0.0006</b>	0.0016	0.9629	0.8454
R_square	<b>0.2715</b>	0.1891	0.0016	0.0008
root_mean_square_error	<b>1.3935</b>	1.4548	1.6313	1.6149
max_viability at optimum (%)	<b>98.8</b>		NS 98.2	
optimum AU or rank	<b>2626.6</b>		NS 31.9	
<b>20 hours, 2.5M KCl</b>				
probability > F	<b>&lt; 0.0001</b>	< 0.0001	<b>0.0055</b>	0.6023
R_square	<b>0.4286</b>	0.3138	<b>0.1987</b>	0.0057
root_mean_square_error	<b>7.0949</b>	7.6940	<b>8.4022</b>	9.2615
max_viability at optimum (%)	<b>86.7</b>		<b>86.3</b>	
optimum AU or rank	<b>2662.5</b>		<b>24.4</b>	
<b>48 hours, 2.5M KCl</b>				
probability > F	<b>&lt; 0.0001</b>	0.0003	<b>0.0013</b>	0.9159
R_square	<b>0.3148</b>	0.2371	<b>0.2464</b>	0.0002
root_mean_square_error	<b>7.6281</b>	8.1323	<b>8.1679</b>	9.3096
max_viability at optimum (%)	<b>82.2</b>		<b>82.9</b>	
optimum AU or rank	<b>2622.3</b>		<b>25.7</b>	
<b>72 hours, 2.5M KCl</b>				
probability > F	<b>0.0010</b>	0.0033	<b>0.0062</b>	0.8464
R_square	<b>0.2556</b>	0.1660	<b>0.1943</b>	0.0008
root_mean_square_error	<b>9.9877</b>	10.4608	<b>10.3903</b>	11.4501
max_viability at optimum (%)	<b>73.5</b>		<b>74.3</b>	
optimum AU or rank	<b>2586.8</b>		<b>25.1</b>	
<b>96 hours, 2.5M KCl</b>				
probability > F	<b>0.0060</b>	0.0018	<b>0.0065</b>	0.0954
R_square	<b>0.1956</b>	0.1862	<b>0.1927</b>	0.0569
root_mean_square_error	<b>8.4186</b>	8.3789	<b>8.4338</b>	9.0201
max_viability at optimum (%)	<b>71.7</b>		<b>71.0</b>	
optimum AU or rank	<b>3389.8</b>		<b>21.3</b>	

**120 hours, 2.5M KCI**

probability > F	0.0791	0.0413	<b>0.0004</b>	0.0037
R_square	0.1023	0.0839	<b>0.2859</b>	0.1625
root_mean_square_error	8.5666	8.5636	<b>7.6405</b>	8.1881
max_viability at optimum (%)	NS 67.7		<b>74.7</b>	
optimum AU or rank	NS 1679		<b>18.1</b>	

**144 hours, 2.5M KCI**

probability > F	0.3473	0.1675	<b>0.0047</b>	0.0501
R_square	0.0440	0.0393	<b>0.2038</b>	0.0776
root_mean_square_error	9.6837	9.6059	<b>8.8377</b>	9.4123
max_viability at optimum (%)	NS 61.9		<b>68.3</b>	
optimum AU or rank	NS 1481.3		<b>20.4</b>	

**168 hours, 2.5M KCI**

probability > F	0.1785	0.3433	<b>&lt;0.0001</b>	< 0.0001
R_square	0.0707	0.0187	<b>0.5733</b>	0.4911
root_mean_square_error	12.3795	12.5879	<b>8.3885</b>	9.0652
max_viability at optimum (%)	NS 56.2		<b>68.4</b>	
optimum AU or rank	NS 2077		<b>9.7</b>	

**24 hours, 3M KCI**

probability > F	0.0107	0.0292	<b>&lt; 0.0001</b>	< 0.0001
R_square	0.1757	0.0952	<b>0.5254</b>	0.2980
root_mean_square_error	11.8963	12.3332	<b>9.0267</b>	10.8635
max_viability at optimum (%)	71.7		<b>65.0</b>	
optimum AU or rank	2029.2		<b>18.1</b>	

**48 hours, 3M KCI**

probability > F	0.0294	0.0140	<b>&lt; 0.0001</b>	0.0003
R_square	0.1394	0.1193	<b>0.5382</b>	0.2402
root_mean_square_error	12.8903	12.9029	<b>9.4420</b>	11.9849
max_viability at optimum (%)	NS 57.1		<b>62.3</b>	
optimum AU or rank	NS 2867.3		<b>19.7</b>	

**72 hours, 3M KCI**

probability > F	0.0519	0.0395	<b>&lt; 0.0001</b>	0.0002
R_square	0.1183	0.0853	<b>0.5459</b>	0.2460
root_mean_square_error	12.4241	12.5218	<b>8.9158</b>	11.3687
max_viability at optimum (%)	NS 51.4		<b>56.9</b>	
optimum AU or rank	NS 2651		<b>19.7</b>	

**Adaptation limit**

probability > F	0.5435	0.2699	<b>0.0002</b>	0.0086
R_square	0.0262	0.0258	<b>0.3099</b>	0.1379
root_mean_square_error	0.1344	0.1330	<b>0.1132</b>	0.1251
max_concentration optimum (M)	NS 2.8		<b>2.8</b>	
optimum AU or rank	NS -95.6		<b>31.2</b>	



671 **Table 5. Clustering statistics used to rank signaling behavior.**

672 Statistics showing the fraction of 17,000 permutations in which strains were clustered with at  
 673 least 50% of the other strains in each mean cluster. These data were used to rank total  
 674 signaling behaviors from most cautious (1) to most reckless (50) based on the fraction of time  
 675 each strain was associated with its mean cluster (characteristic of that cluster). See Figure 2.  
 676

Rank	Cluster	Strain	MC0	MC1	MC3	MC2	MC5	MC4
1	MC0	W455	0.8484	0.1516	0	0	0	0
2	MC0	W167	0.8365	0.1635	0	0	0	0
3	MC1	W219	0.6375	0.3625	0	0	0	0
4	MC1	W217	0.5536	0.4460	0.0004	0	0	0
5	MC1	W027	0.5214	0.4755	0.0028	0.0002	0	0
6	MC1	W042	0.4850	0.4892	0.0191	0.0044	0.0023	0.0001
7	MC1	W235	0.1976	0.5532	0.2266	0.0226	0	0.0002
8	MC1	W340	0.1700	0.5803	0.2354	0.0142	0	0
9	MC1	W454	0.3355	0.6610	0.0034	0	0	0
10	MC1	W134	0.1686	0.7376	0.0821	0.0117	0	0
11	MC1	W276	0.1617	0.7643	0.0658	0.0083	0	0
12	MC1	W294	0.1692	0.7834	0.0440	0.0034	0	0
13	MC1	W157	0.1195	0.7851	0.0866	0.0088	0	0
14	MC1	W202	0.1671	0.7855	0.0446	0.0027	0	0
15	MC1	W238	0.1337	0.8048	0.0580	0.0036	0	0
16	MC1	W035	0.1293	0.8086	0.0572	0.0050	0	0
17	MC1	W248	0.1494	0.8331	0.0172	0.0003	0	0
18	MC3	W130	0.0003	0.0671	0.7020	0.2307	0	0
19	MC3	W136	0	0.0092	0.6572	0.3334	0.0002	0
20	MC3	W203	0.0025	0.1348	0.6410	0.2214	0.0002	0
21	MC3	W285	0.0003	0.0806	0.6245	0.2924	0.0022	0
22	MC3	W163	0.0011	0.1474	0.6228	0.2285	0.0002	0
23	MC3	W206	0	0.0036	0.6203	0.3747	0.0014	0
24	MC3	BY41	0	0.0123	0.6102	0.3768	0.0008	0
25	MC3	W041	0.0002	0.0233	0.5625	0.4090	0.0050	0
26	MC3	W343	0.0012	0.0432	0.5522	0.3910	0.0123	0.0002
27	MC3	W292	0.0201	0.1962	0.4883	0.2893	0.0062	0
28	MC3	W189	0.0001	0.0205	0.4757	0.4715	0.0319	0.0003
29	MC3	W211	0	0	0.3698	0.5572	0.0696	0.0033
30	MC2	W245	0	0	0.2579	0.6898	0.0523	0
31	MC2	W291	0	0	0.2211	0.6786	0.0994	0.0009

32	MC2	W164	0	0	0.1517	0.6601	0.1852	0.0031
33	MC2	W249	0	0	0.3349	0.6417	0.0233	0.0001
34	MC2	W166	0	0	0.3372	0.6407	0.0220	0.0001
35	MC2	W179	0	0.0002	0.3569	0.6212	0.0217	0
36	MC2	W244	0	0	0.1478	0.6160	0.2225	0.0137
37	MC2	W173	0	0.0003	0.3801	0.6005	0.0188	0.0002
38	MC2	W215	0	0.0012	0.3162	0.6000	0.0815	0.0011
39	MC2	W037	0	0	0.0714	0.5308	0.3863	0.0115
40	MC2	W255	0	0.0011	0.4771	0.5141	0.0077	0
41	MC2	W050	0	0	0.0567	0.4672	0.4417	0.0343
42	MC5	W044	0	0	0.0021	0.0728	0.8501	0.0750
43	MC5	W195	0	0	0.0019	0.0744	0.8501	0.0736
44	MC5	W301	0	0	0.0029	0.0882	0.8203	0.0887
45	MC5	W150	0.0001	0.0004	0.0006	0.0414	0.7978	0.1598
46	MC5	W033	0	0	0	0.0279	0.7196	0.2525
47	MC5	W153	0	0	0	0.0181	0.6545	0.3274
48	MC4	W282	0	0	0	0	0.0596	0.9404
49	MC4	W242	0	0	0	0.0002	0.1477	0.8521
50	MC4	W178	0	0	0	0.0017	0.1697	0.8286

677

678 **Figures**

679 (High resolution figures available at <https://figshare.com/s/222fd592f52f59d5d4fb> )

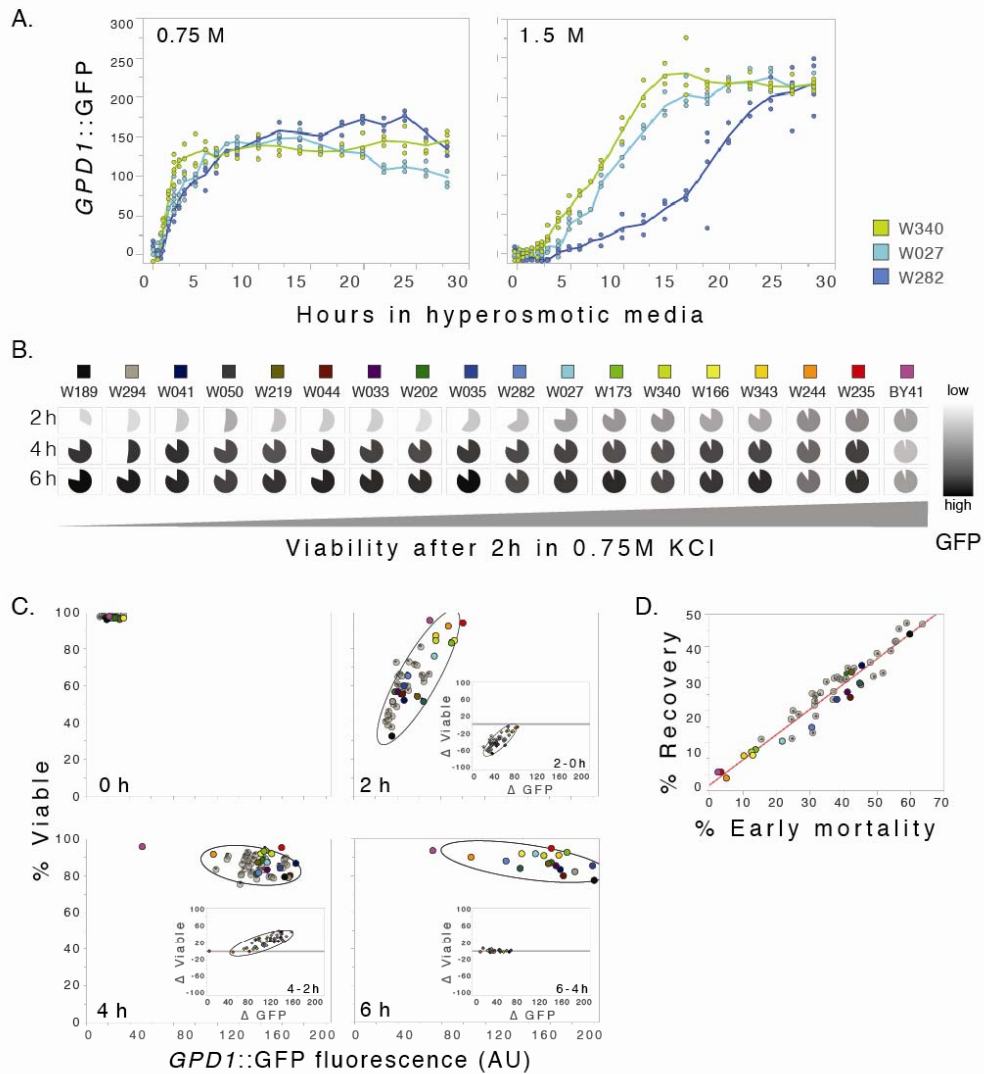
680

681 **Figure 1. Rate of change in osmotic stress signaling with negative feedback predicts**  
682 **survival and robust recovery of exponential cultures in moderate hyperosmotic stress.**

- 683 A. Time course of mean accumulated *GPD1::GFP* fluorescence in exponential cultures  
684 exposed to 0.75 and 1.5 M KCl. Each point represents an independent experimental  
685 replicate; curves connect strain means at each time (minimum of 3 replicates per time).  
686 In the absence of stress, all strains had high steady-state viability (propidium iodide dye  
687 exclusion; range 96.3 – 98.7%; mean 97.6%) and relatively low mean GFP fluorescence  
688 indicating low background activity of HOG pathway signaling through the *GPD1*  
689 promoter and low *GPD1::GFP* accumulation (range 12.7 – 34.8 AU; mean 18.8 AU).  
690 *GPD1::GFP* accumulation reached a steady state by 4 to 6 hours in 0.75 M KCl.
- 691 B. Pie charts show relative changes in mean viability (shaded area), mortality (white area)  
692 and *GPD1::GFP* accumulation (opacity level) of 18 representative strains after 2 hours in  
693 0.75M KCl with strains ordered by increasing viability at 2 hours. Across all 50 strains 2-  
694 hour viability was proportional to the 2-hour viability of non-disrupted controls with two  
695 intact copies of the *GPD1* gene ( $R^2 = 0.7085$ ;  $P < 0.0001$ ; not shown).
- 696 C. Relationship between mean *GPD1::GFP* accumulation (AU) and viability in mid-  
697 exponential cultures exposed to 0.75 M KCl for 0, 2, 4, and 6 hours (h). Each data point  
698 represents an average of at least three replicates per strain and time (~10,000 cells/  
699 sample). The ellipses indicate correlations between viability and fluorescence at  $\alpha =$   
700 0.95. The inserts show relationships between changes in *GPD1::GFP* and viability over  
701 each time interval.
- 702 D. Negative feedback drove robust recovery of steady-state viability after 4 hours in 0.75 M  
703 KCl (robust perfect adaptation; see (Muzzey et al., 2009)). Linear regressions of  
704 recovery at 4 hours – recovery = (0.7670) early mortality + 3.49 ( $R^2 = 0.9351$ ;  $P < 0.0001$ ;  
705 50 strains, shown) and at 6 hours – recovery = (0.7670) early mortality + 3.43 ( $R^2 =$   
706 0.9852;  $P < 0.0001$ ; 18 strains). Integral feedback control would assure and be assured  
707 by perfect adaptation of stress responses, water balance and steady state viability  
708 (manuscript in preparation; bioRxiv <http://dx.doi.org/10.1101/045682>). Note that due to  
709 the persistence of dead cells in short term cultures (early mortality), 100% recovery of  
710 steady-state viability (slope = 1) is not expected over the course of the experiment. The  
711 data are fit well by a model whereby dead cells remain and surviving cells in all strains  
712 undergo 3 cell divisions (not shown).

713

Figure 1

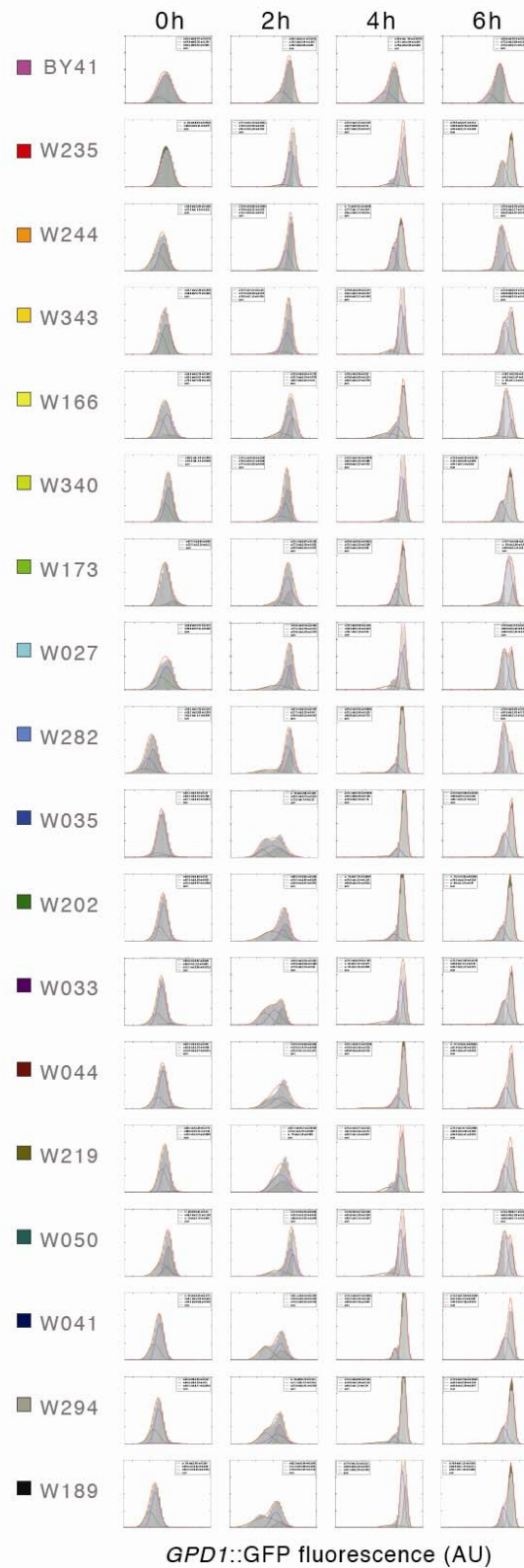


714  
715

716 **Figure 1–figure supplement 1. Mean *GPD1::GFP* accumulations accurately track the rate**  
717 **of osmotic stress signaling in exponential cultures.**

718 Representative distributions of cells from exponential cultures exposed to 0.75 M KCl for the  
719 times shown were generally monomodal and well-approximated by mean values. Learned  
720 frequency distributions of *GPD1::GFP* accumulation (AU) with mean ( $\mu$ ), standard deviation  
721 (std), and weight ( $w$ ; the fraction of cells in each distribution) shown in boxes (zero-weighted  
722 distributions not shown). Sum (red) shows the cumulative fit of the 4 learned Gaussians.  
723 *GPD1::GFP* values were normalized across all strains for comparison. The 18 representative  
724 strains are color-coded as in Figure 1B.  
725

Figure 1  
Supplement 1

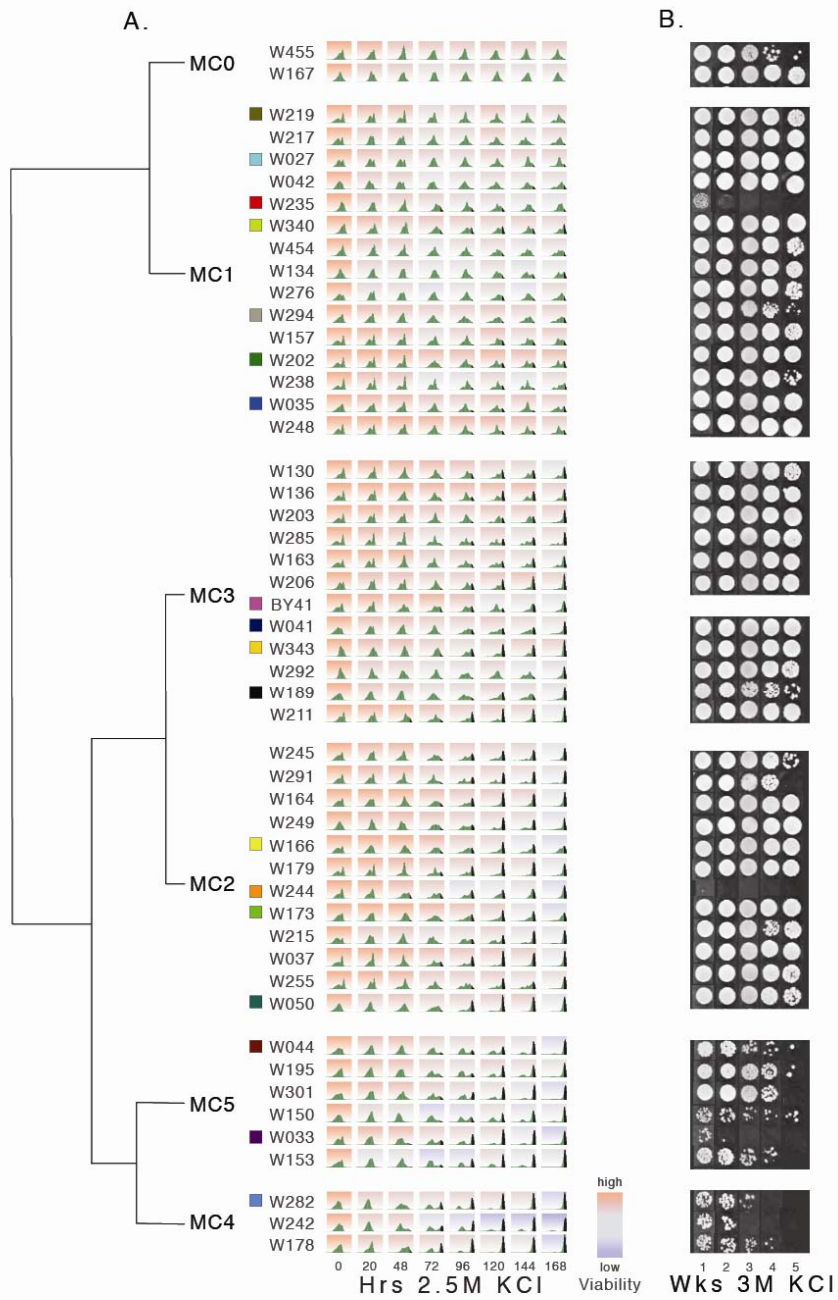


727 **Figure 2. Continuous variation in survival and rates of accumulation of *GPD1::GFP***  
728 **fluorescence of postdiauxic cultures during severe hyperosmotic osmotic stress.**

- 729 A. Strains were clustered (MC0 – MC5) and ranked according to their rates of accumulation  
730 of *GPD1::GFP* fluorescence (see Table 5 and methods). A representative distribution of  
731 *GPD1::GFP* accumulation (green) and relative survival red (99.7% viability) to blue  
732 (11.7% viability) is given for each strain and time point (4-15 fold replication).  
733 Distributions of cells above the 89<sup>th</sup> percentile (top 11%) are shown in black. Ranking  
734 was sequential from 1 (top) to 50 (bottom). Prior to osmotic challenge (0 hours in 2.5 M  
735 KCl) steady-state viabilities were uniformly high (range 93.0 – 99.6%; mean 98.2%).  
736 Strains are color-coded as in Figure 1C for comparison of exponential and post-diauxic  
737 cultures.
- 738 B. Relative viability of post-diauxic cultures (WXXX.BY01 controls) incubated in 3 M KCl  
739 before plating on iso-osmolar media. Platings were re-ordered according to the ranked  
740 signaling behavior given in Figure 2A.

741

Figure 2



742

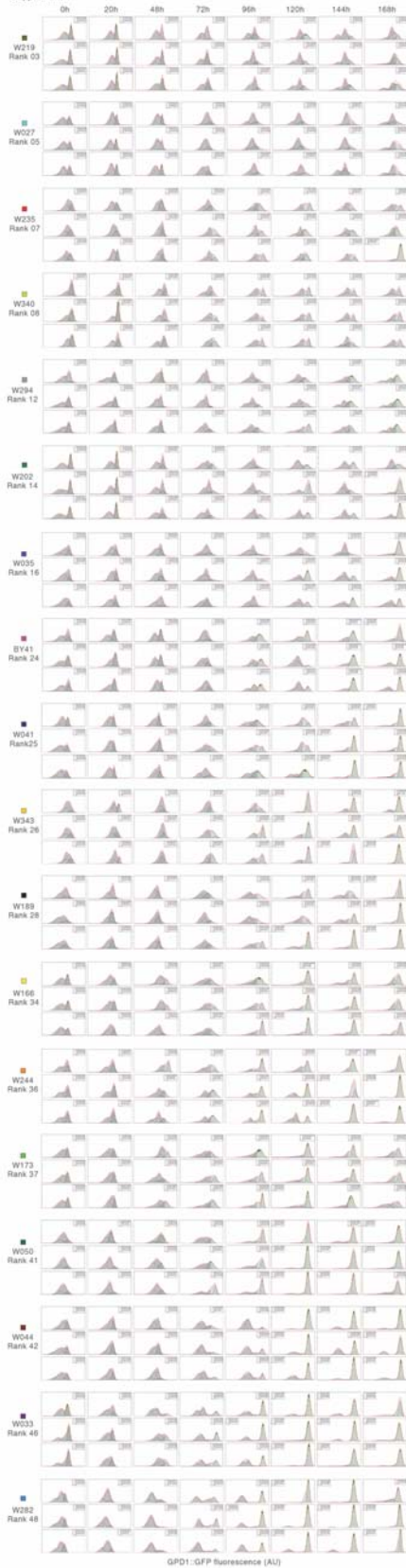
743

744 **Figure 2–figure supplement 1. Reproducible rates of *GPD1::GFP* accumulation in post**  
745 **diauxic cultures during extreme hyperosmotic stress.**

746 Representative replicates of learned distributions of *GPD1::GFP* accumulation in post-diauxic  
747 cultures exposed to 2.5 M KCl for the times shown. Mean ( $\mu$ ), standard deviation (std), and  
748 weight ( $w$ ; the fraction of cells in each distribution) are given (zero-weighted distributions not  
749 shown). Sum (red) shows the cumulative fit of the 4 learned Gaussians. The 18 strains shown  
750 are color-coded as in Figure 1B.

751

Figure 2  
Supplement 1



753 **Figure 2-figure supplement 2. Rank predicts rate of *GPD1::GFP* accumulation.**

754 Strains were exposed to 2.5 M KCl for increasing times shown and ordered according to rank.

755 The average percent of cells in each strain above a threshold set at the top 11% of

756 accumulation of *GPD1::GFP* normalized across all post-diauxic cultures. Significant P-values for

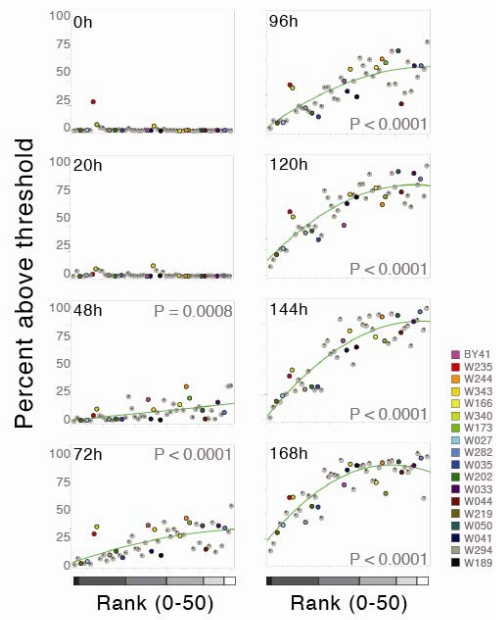
757 2<sup>nd</sup> order quadratic fits of the data are shown (JMP, SAS Institute; N=50 strains). The number of

758 strains in each mean cluster is indicated with increasingly lighter grey scale in their order of

759 'cautious' to 'reckless' signaling: 2 strains (MC0), 15 (MC1), 12 (MC3), 12 (MC2), 6 (MC5), 3

760 (MC4). The 18 representative strains are color-coded as in Figure 1B.

Figure 2  
Supplement 2



762 **Figure 2–figure supplement 3. Regrowth after static viability and survival in extreme**  
763 **hyperosmotic stress.**

764 Raw data used for montage for Figure 2B shown as plated. Post-diauxic cultures were  
765 incubated for up to 5 weeks in 3 M KCl and then plated on iso-osmolar media.

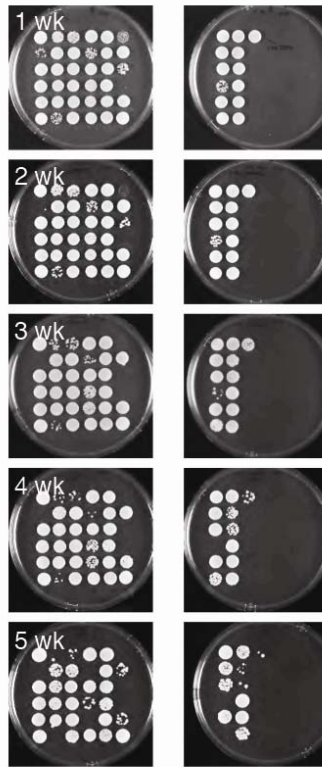
766

767 **Plate key**

	1	2	3	4	5	6
A	W027.BY01	W044.BY01	W153.BY01	W173.BY01	W203.BY01	W235.BY01
B	W033.BY01	W050.BY01	W157.BY01	W178.BY01	W206.BY01	W238.BY01
C	W035.BY01	W130.BY01	W163.BY01	W179.BY01	W211.BY01	W242.BY01
D	W037.BY01	W134.BY01	W164.BY01	W189.BY01	W215.BY01	W244.BY01
E	W041.BY01	W136.BY01	W166.BY01	W195.BY01	W217.BY01	W245.BY01
F	W042.BY01	W150.BY01	W167.BY01	W202.BY01	W219.BY01	W248.BY01
	1	2	3			
A	W249.BY01	W292.BY01	W455.BY01			
B	W255.BY01	W294.BY01				
C	W276.BY01	W301.BY01				
D	W282.BY01	W340.BY01				
E	W285.BY01	W343.BY01				
F	W291.BY01	W454.BY01				

768

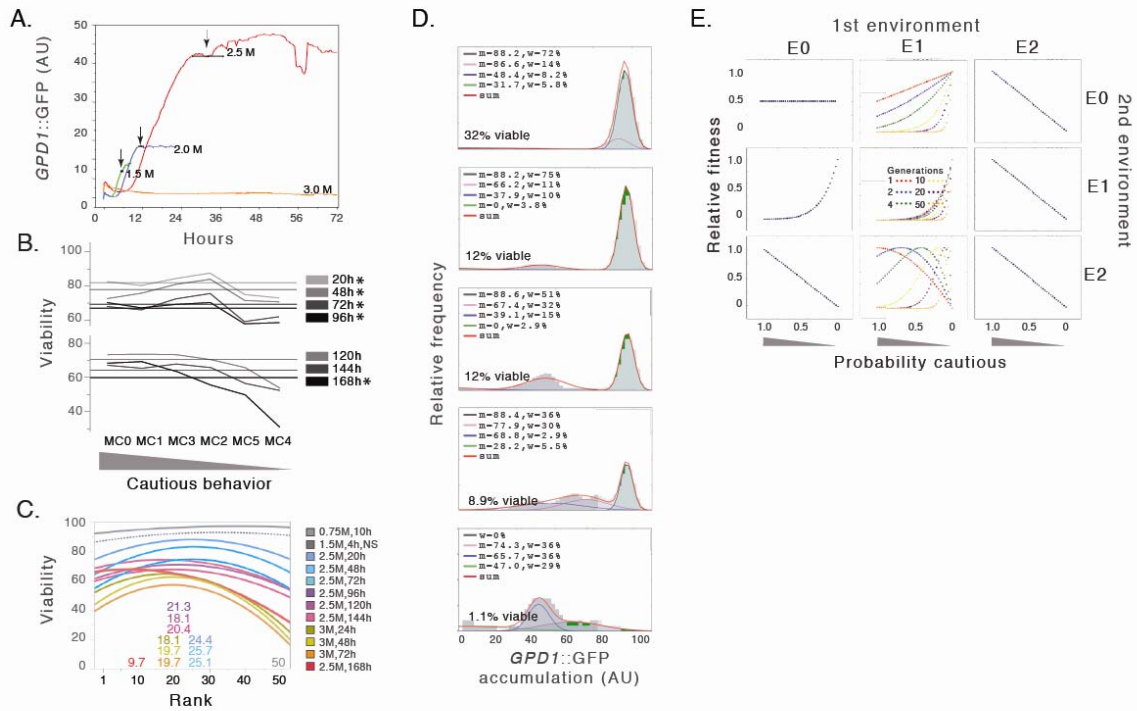
Figure S2



770 **Figure 3. Modeling a heritable probability of cautious behavior (bet hedgers) produces**  
771 **observed variation in relative fitness and survival.**

- 772 A. The most cautious behavior (static viability) of post-diauxic cells from strain W027  
773 exposed to 3 M in microfluidic chambers. Individual cell behaviors mirror population  
774 behaviors measured by flow cytometry – e.g longer lag periods and increased  
775 accumulations of *GPD1::GFP* with increasing osmotic stress. Colored traces indicate  
776 accumulated fluorescence (AU X 10<sup>-2</sup>) in representative cells at 1.5 (green), 2.0 (blue),  
777 2.5 (red) and 3.0 M KCl (yellow). Arrows indicate average time to the first cell division  
778 +/- standard deviations.
- 779 B. Mean cluster predicts viability in different osmotic environments. Average viabilities  
780 among mean clusters for post-diauxic cultures in 2.5 M KCl for indicated times.  
781 Horizontal lines show overall average viability at each time point across all 50 strains.  
782 The numbers of strains in each mean cluster are 2 (MC0), 15 (MC1), 12 (MC2), 12  
783 (MC3), 3 (MC4), 6 (MC5; see Figure 2). Asterisks indicate significance at the  $\leq 0.05$  level  
784 by ANOVA or, where appropriate because variances were unequal, Welch's ANOVA  
785 (JMP statistical software, SAS Institute, Cary, NC).
- 786 C. Rank predicts viability in different osmotic environments. Shown are the best-fit curves  
787 for viability by rank in each of the environments listed (2<sup>nd</sup> order quadratic relationships;  
788 Table 4). The optimal signaling strategy (rank) shifted from higher (50; most reckless) to  
789 lower (most cautious) as the environment became progressively more severe. Dashed  
790 lines indicate the relationship between rank and viability was only marginally significant  
791 in that environment.
- 792 D. Cells with the most aggressive signaling began to die after long periods in severe stress  
793 leaving increasing fraction of cells with lower *GPD1::GPF* accumulations. Shown are  
794 distributions of accumulated *GPD1::GFP* fluorescence (AU) and viability in replicate  
795 cultures of W242 (rank 49) in 5 replcate cultures after 168 hours in 2.5 M KCl. Mean (x),  
796 standard deviation (std), and weight (w; the fraction of cells in each distribution) are  
797 given. Sum (red) shows the cumulative fit of the 4 learned Gaussians.
- 798 E. A simple bet hedging model with heritable proportions of cautious and reckless cells  
799 produces observed variation in survival. Bet hedging strategy P was defined as the  
800 probability of cautious cells for  $0 \leq P \leq 1$ . Relative fitness was measured for all strategies  
801 after 10 generations in each environment. All nine possible 2-state environmental shifts  
802 between three general osmotic stress environments were considered: permissive (E0; all  
803 cells grow equally well), restrictive (E1; reckless cells divide, cautious cells survive  
804 without dividing), and killing (E2; reckless cells die, cautious cells survive without cell  
805 division). Intermediate strategies ( $0 < P < 1$ ; i.e. bet hedging) were most fit only when the  
806 environment shifted from moderate to more severe (E1 -> E2). When E1 was the first  
807 environment, the optimum strategy P depended on generation number.  
808

Figure 3



810 **Movie Legends**

811

812 **Movie 1.** Exponential W027 cells seeded with a single post diauxic cell of the same genotype  
813 (box). Media was switched to 1.5M KCl at time 0, GPD1::GFP fluorescence is shown in green.  
814 Time stamp shown in upper right.

815

816 **Movie 2.** Post-diauxic W027 cells exposed to 1.5 M KCl, GPD1::GFP fluorescence is shown in  
817 green. Time stamp shown in upper right.

818

819 **Movie 3.** Post-diauxic W027 cells exposed to 2.5 M KCl, GPD1::GFP fluorescence is shown in  
820 green. Time stamp shown in upper right.

821

822 **Bet hedging model**

823

824 Annotated code for our model of bet hedging with heritable probability of binary, cautious versus  
825 reckless bet hedging is publicly available (<https://figshare.com/s/2c03544aef0c40cc86c2>). The  
826 bet hedging ‘strategy’  $P$  was defined as the heritable probability of cautious cells for  $0 \leq P \leq 1$ .  
827 Nine possible 2-state environmental shifts between three general osmotic stress environments  
828 were considered: permissive (E0; all cells grow equally well), restrictive (E1; reckless cells  
829 divide, cautious cells survive without dividing), and killing (E2; reckless cells die, cautious cells  
830 survive without cell division). The relative fitness of representative strategies (0, 0.1, 0.2, ...1.0;  
831 number of surviving cells in each strategy divided by the total number of surviving cells across  
832 all strategies) was calculated after 10 generations in each environment except as shown on  
833 Figure 3c. For simplicity, the natural attrition of older cells (death and disappearance) and rates  
834 of cell division were assumed to be equal for all strains. Results were independent of the  
835 number of generations in the first environment except as shown when E1 was the first  
836 environment.

837

838

839 **Databases and linked archives**

840 Flow cytometry database (annotated)

841 <https://figshare.com/s/52ef966b16cba7f41d7f>

842

843 Python script for bet hedging model

844 <https://figshare.com/s/2c03544aef0c40cc86c2>

845

846 Figure 1–figure supplement S1 complete data set

847 <https://figshare.com/s/8b709fd16cccbabc2a5a>

848

849 Figure 3–figure supplement S3 complete data set

850 <https://figshare.com/s/8147275b62eb8d4db6bf>

851

852 Excel file with tables and raw data

853 <https://figshare.com/s/00a7bf31d2791922f1d8>

854